Multi-decadal shoreline mobility of a managed sandy tidal coast (Normandy, France): Behavioural variability in a context of sea-level rise and increasing storm intensity

Franck Levoy, Olivier Monfort, Edward J. Anthony

Version of Record: https://www.sciencedirect.com/science/article/pii/S2352485523001627
Manuscript_1a37a50416a0c018c9fe5a72f268a9c6

Multi-decadal mobility of a managed sandy tidal coast (Normandy, France): behavioural variability in a context of sea-level rise and increasing storm intensity

Franck LEVOY[a], Olivier MONFORT[a], Edward J. ANTHONY[b]

[a]: Université de Caen Normandie, Esplanade de la Paix, CS 14032, 14032 Caen Cedex, France, franck.levoy@unicaen.fr, olivier.monfort@unicaen.fr.

[b]: Aix Marseille University, CNRS, IRD, INRAE, Coll France, CEREGE, Aix-en-Provence, France, anthony@cerege.fr

Abstract:

A unique dataset of 27 years of shoreline changes along the western coast of Cotentin Peninsula (Normandy, France) with a high temporal resolution (about 60 fields surveys) provides an opportunity to analyse the space and time variability of a tidal sandy wave-exposed shoreline and to identify the main drivers of this variability. Spatially, as often observed around the world, this coast shows a clear balance between erosional and accretionary sectors. Maximum shoreline retreat and mean annual erosional rates are, however, greater by a factor of two than maximum and mean accretion rates, with hotspots mainly observed in the vicinity of tidal inlets. A cluster analysis highlighted nine groups of shoreline behaviour that show important contrasts, depending on locations, between erosional and accretionary trends. Linear trends over the nearly three decades of monitoring are uncommon and reverse trends are frequent. Clear divergences in behaviour were observed over the same time periods depending on location, e.g., erosion and accretion can be contemporaneous as can accretion and stability, independently of the antecedent multi-annual trends. Ebb delta zones show heterogeneous patterns, and survey locations belonging to the same clusters appear spatially scattered. The temporal shoreline behaviour can be linked to combinations of high wave energy and high spring tides only for at best 37.5% of the survey locations, and this only over the last decade. No obvious link with mean sea-level rise and the 18.6 y lunar tidal cycle was observed. However, as in the case of wave activity, these external drivers can often be masked by local factors such as inlet dynamics or/and anthropogenic influences (essentially shoreline engineering). Further insight on sand supply and beach elevation changes is necessary to improve the understanding of the main factors driving space and time variability in shoreline mobility, and it is expected that sea-level rise in the future will be of increasing concern, with important, potentially negative, implications for shoreline mobility on the low sandy sectors of the Normandy coast.

Keywords: tidal sandy coast, multi-decadal shoreline change, sea-level rise, wave energy flux, NAO index, WEPA index, coastal engineering.

1 Introduction

Forecasting shoreline changes has become a major challenge for society and coastal managers with the increasing need to identify the drivers of change and consider the most appropriate solutions to counter eventual hazards. Shoreline recession is observed along many sandy coasts around the world. Nearly three decades ago, Bird (1985) reported 20% of the world's coasts as sandy, of which more than 70% were eroding, with only 10% showing progradation, and 20-30% stability. Using satellite data on shoreline changes since 1984 at a global scale, Luijendijk et al. (2018) showed that about 31% of the world's ice-free shorelines are sandy

and 24% of them eroding at a rate exceeding 0.5 m/y, while 28% are accreting and 48% are stable. At a regional scale, several studies have underlined variability in both spatial and temporal contemporary shoreline mobility (Leatherman and Douglas, 2003; Pye and Blott, 2008; Del Río et al., 2013; Hapke et al., 2016; Burningham and French, 2017; Konlechner et al., 2020). This variability suggests the influence of a large range of factors. Sediment sources and sinks and longshore and cross-shore gradients in sediment transport have been considered as primary controls and their importance emphasised (e.g., Stive et al. 2002; Stive, 2004; Hapke et al., 2010; Anthony and Aagaard, 2020). The influence of fragmentation of river-to-coast and alongshore sediment connectivity has emerged as an important criterion in engendering time and space variations in shoreline mobility (e.g., Besset et al., 2019). Internal dynamic mechanisms can also influence sediment availability. Lazarus and Murray (2007) observed, for instance, shoreline regularisation in response to sediment diffusion from gradients in longshore transport. Other driving factors interacting with hydrodynamic conditions have also been identified. Coastal geology and morphology (bathymetry, shoreline orientation, presence of bedrocks and platforms) can be significant controls on shoreline shape and changes (Anthony, 2013; Burningham and French, 2017; Cooper et al., 2020; Sarti et al., 2022), and a primordial parameter in beach morphodynamics (Gallop et al., 2020).

In addition to the overarching condition of sediment availability, the consequences of sea-level rise have been advocated (Vousdoukas et al., 2020) but Cazenave and Le Cozannet (2014) and Cooper et al. (2020) have argued that the local to regional natural and human settings of coastal systems are extremely important in characterizing their response to sea-level rise. Le Cozannet et al. (2014) and Dean and Houston (2016) have claimed that sea-level rise has, thus far, been only a minor contributor to shoreline change along many coasts, but its role appears set to increase and become overarching as the rate of sea-level rise increases (IPCC, 2022). Long-term tidal cycles (Gratiot et al., 2008) and surge water levels (Chaverot et al., 2008), are mentioned as other hydrodynamic factors to be considered, in addition to storm dynamics (Pye and Blott, 2008). At a multi-decadal scale, Feser et al. (2015) analysed storms over the North Atlantic and northwestern Europe and showed particularly increasing activity north of 55°-60°N. Using wave buoy and satellite altimeter measurements combined with numerical wave hindcasts, Castelle et al. (2018a) identified a significant increase in winter wave heights over the last decades in the northeast Atlantic, north of 50°N, potentially a source of perturbation of the stability of sandy shorelines in western Europe. Increases in storm and wave activity are expected to result from climate change (Ranasinghe, 2016), and must be taken into account in forecasts of future shoreline behaviour. Beyond its role in the increase in CO_2 and other GES concentrations in the atmosphere and in major changes in the world's sediment budget and the source-to-coast sediment circuit over the course of the Anthropocene (Syvitski et al., 2022), human activity has directly impacted coasts since time immemorial (Anthony, 2009), notably through engineering implantations ranging from large ports to seawalls, dikes, breakwaters and groynes, and, in more recent times, large nourishment projects.

As a result of this diversity of potential driving factors, regional studies (shorelines >10 km) show, as a general rule, little alongshore and temporal coherence in shoreline behaviour (Del Río et al., 2013; Burningham and French, 2017; Harley et al., 2017; Vos et al., 2019; Konlechner et al., 2020). The interweaving of regional and local factors often clouds perception of the role of any specific forcing factor in determining shoreline changes. This variability in time-space scales of shoreline change is a source of rising concern and is coming under stronger scrutiny by coastal scientists, managers and authorities. Unfortunately, high-

resolution shoreline datasets are not always available (Le Cozannet et al., 2014) to foster progress in knowledge of future shoreline positions suggested by modelling approaches (Le Cozannet et al., 2019; Montaño et al., 2020). The uncertainty regarding future rates of sea-level rise further clouds the problem.

Here, we analyse the behaviour of the sandy west coast of the Cotentin Peninsula, in Normandy, France, between the rocky headlands of Barneville-Carteret and Roc of Granville (Fig. 1), an area characterised by a megatidal range (Levoy et al., 2000, 2001). Shoreline erosion observed after a particularly stormy period in the 1980s incited the regional authorities to initiate a large-scale monitoring scheme of sediment transport and morphological change (Levoy et al., 1994a, 1994b). This monitoring, which started mainly in 1992, is probably the oldest in France with now three decades of data acquisition at a regional scale, and with the highest temporal resolution of datasets with a mean of 2 surveys per year and even three per year in the course of the first two decades. The present study focuses on a shoreline stretch of about 70 kilometres (Fig. 1) with a survey duration of 27 years up to 2019.

The high temporal resolution of the shoreline change dataset offers the opportunity of detecting, over a multi-decadal time frame, the influence of the regional hydrodynamic conditions on shoreline mobility, and that of other important, but mainly local, driving factors, such as the effects of inlet dynamics and direct human actions. It is hoped that the approach will contribute to improving the understanding of future changes in a tidal environment, in a context of climate change, in order to better inform management, and eventually foster adaptation of specific policies aimed at protecting the coastal populations, economic activities, and ecosystems of Normandy. The study should also serve as an example for other regional studies on shoreline mobility.

2 Study area

The west Cotentin coast is a low-lying rectilinear sandy system bounding the Channel Islands embayment (Fig. 1) into which debouch several small rivers with inlets locally called ‘havres’ (a term probably derived from the north European word ‘haven’). These inlets are characterised by vigorous tidal activity. The tidal range, considered as ‘megatidal’ (Levoy et al., 2001), decreases from 14.3 m in Granville to 11.9 m towards the north, close to Barneville-Carteret. The tidal wave is dominated by the M2 (semi-diurnal) harmonic. Strong tidal current activity is expressed by mean current velocities reaching 1 $m.s^{-1}$ at high tide on the lower part of beaches and up to 3 $m.s^{-1}$ in the inlets. The offshore wave regime is forced by dominantly westerly local and synoptic winds. Southwesterly to northwesterly winds are active in winter and generate waves with periods of 4-6 s. The maximum annual significant wave height varies from 4.2 m at Les Trois Grunes about 10 km off Barneville-Carteret to 2.8 m at Videcoq, off Granville (Fig. 1). The propagation of longer Atlantic swell is impeded by the shallow shoreface bathymetry, and by the numerous low rocky platforms, islets, shoals, and tidal deltas (Fig. 1) which also locally modify the wave propagation patterns. The embayment is, thus, dominated by short-fetch waves with a negative height gradient from north to south and from west to east.

Figure 1

Sediment circulation along the west Cotentin is longshore-dominated (Levoy, 1994; Levoy et al., 1994b; Robin et al., 2007, 2009a, 2020; Fruergaard et al., 2020), and responsible for the formation of seven major sand spits near inlets within a compartment bound by two

protruding rocky headlands, respectively at Flamanville in the north and Granville in the south (Fig. 2). However, the residual longshore sand transport shows directional contrasts, especially south of Barneville-Carteret (Fig. 2). The main spits close to the largest tidal inlets are elongated southwards, such as Pointe d'Agon near Regnéville inlet, and Pointe du Banc (Fig. 2), near Lessay inlet. Sediment transport northward is also evident from the distal-tip orientation of the smallest spits (such that of Surville inlet) or that of secondary spits generated by reverse sand transport induced by wave refraction over ebb deltas (Blainville inlet, for instance). These residual sand movements, especially dominant on the upper foreshore (Levoy et al., 2001), reveal the presence of littoral sediment sub-cells (Fig. 2) with transport convergences and divergences (Levoy, 1994), as classically identified on sandy coasts at similar spatial scales.

Figure 2

As on many sandy coasts around the world, numerous coastal defence and beach protection structures against storms have been emplaced in west Cotentin (Fig. 3). Seawalls are the most common structures, built in front of urban settlements and resorts, and mainly consisting of armour stones as in Barneville-Carteret, Porbail, Saint-Germain-sur-Ay, Pirou, Agon-Coutainville, Hauteville-sur-Mer, Saint-Martin-de-Bréhal (Fig. 3). Steep to nearly vertical old dikes of concrete blocks or small dressed stones were built decades ago in Donville-les-Bains and over a short distance in Agon-Coutainville. A second generation of coastal structures, mainly groynes, most of the time perpendicular to frontal rock structures, have often been added to counteract the lowering of the beach at the toe of the seawalls. Experiments have also been conducted with wooden structures (Gouville-sur-Mer, Blainville-sur-Mer), but these systematically failed after a few rough winters.

Close to inlets, canals and dikes have been built mainly to stabilise the main navigational tidal channels as in Barneville-Carteret, Portbail and Regnéville inlets. Other hard cross-shore structures are common and serve to access the beach from a road and to put small boats in the water. About 30 of these structures, with lengths between 40 and 120 m, are identified between Cap de Carteret and Roc de Granville. Beach nourishments have also been carried out to counteract budget deficits (Fig. 3). Except for Barneville-Carteret where a significant initial nourishment of about 130,000 m^3 of sand was carried out in 1994, their volumes are low, generally less than 10,000 m^3 per year. Dune-front nourishments have also been implemented in recent years to counter retreat caused by major storms (e.g., Storm Eleanor in 2018), especially at the ends of seawalls, where active erosion is generally observed. Volumes of a few thousands of cubic metres are deposited at the foot of the eroded dune front to smoothen the sub-vertical profile caused by erosion. These nourishments are very vulnerable to erosion and often have a short life time.

Figure 3

3 Methods

The monitoring system consisted of a combination of measurements of shoreline mobility over time, based, initially, on field topographic measurements (1992-2008), and then LiDAR data (2009-2019). The data obtained were subjected to cluster analysis to identify groups of shoreline locations on the basis of their mobility patterns, especially over time. These were then compared with available data on sea level, waves and storms. This methodological procedure is presented in the following sub-sections.

3.1 Shoreline surveys

- **Field topographic measurements**

The beach and shoreline surveys in Normandy were inspired in part by the JARKUS coastal monitoring programme in the Netherlands (e.g. Wijnberg and Terwindt, 1995; Guillen et al. 1999; Kroon et al., 2008). From 1992 to 2008, beach morphology and shoreline locations were determined from topographic measurements at low tide using an electronic theodolite and an infrared-ray distance-metre. This rather time-consuming method was used to survey cross-shore profiles from the dunes or coastal defenses to the low tidal zone during spring tides. There is a variety of definitions of the shoreline (Boak and Turner, 2005) and the proxy used depends on the topic of study. In the Cotentin study, the dune vegetation line marking the contact with bare upper beach sand was selected as the shoreline marker. This line can be identified visually from aerial photographs at the top of an eroded dune cliff as well as along new embryonic dunes. Its location was extracted from topographic measurements by calculating the horizontal distance between the shoreline and wooden ground markers (benchmarks or poles) driven deep in the beach sand.

Overall, 64 wooden benchmarks were installed from autumn 1990 to summer1991 along about 70 km of sandy shoreline. 27 benchmarks were located in front of an ebb delta and 37 outside the ebb delta systems. With an average distance of 0.76 km between two benchmarks, the spatial resolution of this network seems low in comparison to that of the JARKUS programme. However, between 1992 and 2008, 52 field surveys were carried out, i.e., about 3 per year, thus enabling fine-scale monitoring of the seasonal shoreline variability. In addition to monitoring of seasonal shoreline changes, the 1992-2008 dataset also enabled identification of major storm impacts compared to studies using just vertical aerial photographs, which are generally sparse in terms of temporal coverage, or of mean annual shorelines extracted from satellite data as in recent studies (e.g. Luijendijk et al., 2018; Mentaschi et al., 2018). In the field, the estimated accuracy of the horizontal distance between the benchmark and the shoreline, i.e. dune crest for dune fronts in erosion, is about ±0.15 m. For dune fronts showing accretion, sometimes with embryonic features, the accuracy is lower. In these cases, the vegetation line can be discontinuous and the shoreline more difficult to locate exactly in the field. The estimated accuracy is nevertheless good, close to ±0.3 m.

- **LiDAR data**

Airborne LiDAR has been in regular use in the study of high-resolution topographic changes along the coast of Normandy since February 2009 (Levoy et al., 2013; Montreuil et al., 2014; Levoy et al., 2017; Pellerin Le Bas and Levoy, 2018; Levoy et al., 2019; Robin et al., 2020). The generated datasets were acquired between 2009 and 2017 within the framework of the CLAREC project (French acronym for *Contrôle par Laser Aéroporté des Risques Environementaux Côtiers*) (see Levoy et al., 2013, for technical details). Since 2017, the COZULIT project (acronym for *Coastal Zone Changes and Risks Using LiDAR Technology*), successor of the CLAREC project, now enables acquisition, on an annual basis, of topographic data along the Normandy coast. In 2016, another project (ROLNP) enabled the acquisition of topo-bathymetric data using a Leica HawkEye III.

The LiDAR data acquired enable the generation of digital elevation models (DEMs) with a 1 m-grid size. The X and Y coordinates are relative to the Lambert 93 projection system, and

the height, Z, refers to the IGN reference level (French Ordnance Datum), which is close to the mean sea level. The LiDAR data used for the present study, collected between 2009 and 2019, are shown in Tab. 1.

Table 1

While improvements in LiDAR data processing enable extraction of some classic shoreline markers such as the dune crest (Stockdon et al., 2009) or foot (Crapoulet et al., 2017; Le Mauff et al., 2018; Lerma et al., 2019), for incipient foredunes without a clear scarp, the shoreline limit is difficult to locate, and manual corrections are needed. LiDAR data are still not liable to provide a universal proxy of shoreline position, while an elevation reference for the static high-water level appears more relevant because it is the same indicator for erosion or accretion, with the same degree of accuracy, and does not require subjective operations to extract it (Levoy et al., 2016). Given the very large tidal range along the west Cotentin coast, the Highest High-Water Level (HHWL) appears to be the most suitable shoreline proxy based on LiDAR topographic data. A good agreement is observed between the annual velocity changes for the HHWL and the vegetation limit measured in the field for a large set of values, with a slope close to 1 and a correlation coefficient of 0.98 (significant at the 99% level). The changes measured by the two proxies can be considered as coherent in the course of the study period and enable a continuous analysis of shoreline changes. Due to the vertical accuracy of the LiDAR data (0.10 m) and of the slopes around the Highest High-Water level, the estimated mean horizontal accuracy of the shoreline location using these data is about 2.2 m.

- **Cluster Analysis**

A hierarchical cluster analysis enables the classification of coastal behaviour into dominant response groups (Burningham and French, 2017; Burningham and Fernandez-Nunez, 2020), avoiding time, and especially space, interpolations of shoreline data, tricky when the variability is high. A detailed explanation of this method is beyond the scope of this paper. As mentioned by Burningham and French (2017), this tool is sensitive to the choice of the parameters for calculations. In this paper, two types of data were tested: (1) the non-dimensional displacement of the shoreline, and (2) the evolution rate of the shoreline location obtained as the slope of the linear regression line (LRR). An iterative approach involving testing cluster numbers between 3 and 5, numbers of periods between 3 and 8, is used for the data type mentioned above. A tree-view diagram or dendrogram is used to visualise the clusters and the similarities between each item, i.e. the shoreline behaviour at each survey location.

3.2 Sea-level, wave climate and storms

The sea and land levels of the Cotentin Peninsula are derived from three sources: the tide gauge record at Saint-Malo (Fig. 1) between 1993 and 2018 culled from the SONEL database (www.sonel.org), the Permanent Service for Mean Sea Level (PSMSL, (www.psmsl.org)) and the database synthesised by Dodet et al. (2019).

The HOMERE sea-state hindcast database (Boudière et al., 2013) has been used to provide wave data at 8 locations along the study area (Fig. 2). HOMERE is based on the WAVEWATCH III model applied to an unstructured grid covering the English Channel and Bay of Biscay over the period 1994-2016. Hourly time series of significant wave heights,

mean periods, peak energy frequencies and mean directions were archived at each chosen grid node selected in the study area. HOMERE model computations include the influence of parameters affecting wave characteristics in the coastal zone such as fluctuations of the tide level and tidal currents. These parameters are especially important along the west coast of Normandy due to the large tidal range. The HOMERE dataset does not cover the first 16 months and last 29 months of the study period. However, the two gaps represent 16% of the time. The HOMERE data are, however, continuous, over 23 years.

To validate the results of the HOMERE numerical wave database and obtain a continuous time series up to May 2019, field wave measurements were carried out in the central part of the study area, close to Pointe d'Agon (Fig. 2). An electromagnetic InterOcean S4DW current meter (S4), fitted with a pressure sensor, was moored 0.6 m above the seabed, fixed on a stainless-steel frame at a depth of 2.4 m above the lowest water level. A good relationship is observed between the mean wave height of the data obtained at the six HOMERE locations around the S4 position (always < 1 km) and that of the field measurements ($R^2 = 0.99$, significant at the 99% level), thus indicating the robustness of the model outputs despite the different water depths, comprised between -2.25 and +1.15 m.

Despite the shallow shoreface bathymetry and the sheltering provided by the Channel Islands and various shoreface outcrops, the west Cotentin coast is regularly affected by storms. Data on historical storminess over a period extending back to 1962 (well before the commencement of the monitoring project) were collected from various sources - historical accounts, regional archives, news reports and from Météo France, the national meteorological service.

4 Results

4.1 1992-2019 shoreline changes

The non-engineered shorelines (64 locations identified by benchmarks) can be split into two groups, based on their locations relative to an inlet system: very close to an ebb delta and its main channel, or outside this inlet influence (Fig. 2 and 4C). The mean shoreline change in front of an ebb delta (27 benchmarks) is about -7 m and the rms about 67.5 m (Fig. 4B, C), with maximum and minimum values respectively attaining +102.7 m (SW17) and -220 m (SW65). In comparison, the shoreline changes outside ebb delta areas (37 benchmarks) are lower with a mean value of -0.68 m and a rms of about 20.9 m, while the maximum and minimum values reach only +34.1 m (SW85) and -40.4 m (SW42), respectively. These values highlight, near inlets, shoreline mobility over a time span of about three decades that is much larger than along shorelines distant from these inlets. 33 benchmark stations show an accreted shoreline and 31 a situation of erosion between 1992 and 2019, thus highlighting the spatial variability of shoreline behaviour, with erosion quite high at some locations.

Figure 4

Shoreline behaviour is spatially pronounced with zones of dominant accretion (SW75 to SW88) or erosion (for example SW9 to SW12, SW35 to SW47) (Fig. 4A). The heatmap underscores the prevalence of erosion and accretion hotspots mainly close to inlets, especially where shoreline mobility has been high (for example SW32, SW33 and SW34). However, some of these hotspots are sometimes isolated, outside inlet environments, (SW79), but with less intensity. This figure also highlights the large temporal variability of shoreline changes between 1992 and 2019. Negative (erosion) and positive (accretion) changes appeared to be

306 moderate during the first few years, and then increased notably. This mobility pattern has also
307 been complex over time, with, successively, accretion, erosion, light erosion and intense
308 accretion phases at the same location, with often a non-linear trend of shoreline change (for
309 example SW76 on Fig. 4A). Due to the high temporal variability, the rates of shoreline
310 change have been calculated with the End Point Rate (EPR) method (Dolan et al., 1991;
311 Crowell et al., 1997; Thieler et al., 2009) (Fig. 4D). These rates are generally less than 1 m/y
312 (68.7% of yearly rates), with 24 survey locations in erosion and 20 in accretion. The largest
313 changes, close to the inlets, involve accretion of up to 2 and even close to 3 m/y, whereas
314 erosion reaches 6 m/y (SW32), and even 12 m/y (SW65) prior to barrier breaching for these
315 locations. The shoreline changes between 1992 and 2019 can be analysed by considering the
316 main temporal trends over multi-annual to decadal periods. In order to compare the trends for
317 each survey location, all raw data of shoreline change were first normalised.

318 Figure 5 shows the main result of the cluster analysis, i.e. a dendrogram or tree view depicting
319 nine main clusters that regroup several survey locations having the same Shoreline Temporal
320 Change Signature (STCS) at a multi-decadal scale. In all, nine main clusters were identified
321 over the 27-year period. Only two survey locations (SW36 and SW66, Fig. 5I) show some
322 differing multi-annual trends that justify their location in the tree view at the margin of cluster
323 I, close to cluster H. Note also that three other survey locations (SW161, SW162 and SW44)
324 were excluded from the cluster analysis because the surveys there started in 1997 or 1998
325 instead of 1992. However, the temporal shoreline behaviour of these three locations is very
326 similar to that of other clusters (respectively cluster A, D and F). For each survey location, a
327 signature of shoreline temporal changes is obtained showing erosion, accretion or stability
328 phases. Clearly, the temporal shoreline behaviour exhibits important contrasts, depending on
329 location. Linear trends are uncommon, and reverse trends (erosion following accretion or vice
330 versa) are frequent. Clusters A, B C and D show slight to large positive/offshore residual
331 shoreline movements and nearly linear, but time-limited, trends (clusters C and D), or reversal
332 trends (clusters A and C), and sometimes a double-peaked long-term trend (Cluster B).
333 Clusters E and F show weak residual changes but a quasi-inverse behaviour over the study
334 period with, however, respectively, some patterns observed previously such as a smooth peak
335 (maximum) around 2007/2008 (within clusters B and C) and around 1996/1997 (within
336 cluster B). The last three clusters, i.e. G, H and I, typically show large residual shoreline
337 retreat, more or less steep. A peak/accretive period with a maximum also around 1996/1997,
338 as for clusters B and F, is observed for cluster G, showing a long-term trend reversal due to
339 erosion prevailing afterwards. For cluster I, the stable and weak accretive period at the
340 beginning is replaced by a relatively stable period, slightly positive, before a nearly linear
341 intense erosional trend. Cluster H shows, from the survey start, a linear erosional trend
342 culminating in breaches at some locations, followed by a relatively stable shoreline behaviour
343 over the last decade.

344 **Figure 5**

345 Despite large variability in shoreline temporal behaviour, major changes in trends (breaks or
346 inflection points) appear often in the STCSs around 1996/1997, between 2000 and 2001, and
347 early 2008 (Fig. 5). The first inflexion shows a typical reversed shoreline behaviour with a
348 transition between an accretive and an erosive phase. The second marks mainly the beginning
349 of a stable (clusters D, F, G) or accretive phase (clusters A, B, C, E). The last, in early 2008,

shows mainly the beginning of an erosive (clusters E, G, I) or stable phase (clusters A, B, C, H). These breakdowns can be visualised in Fig. 5. No unique shoreline change trend was observed whatever the timescale: erosion, accretion or stability at different locations always coexist. The high temporal variability of shoreline behaviour is underlined again mainly at about a multi-annual time scale (< 10 years).

These results highlight the fact that the three shoreline behavioural modes - erosion, accretion or stability - can be observed during the course of the same period, thus suggesting the influence of various driving factors. The evolutionary trajectories often separate into two branches at the next time step. For example, clusters F and G show a common trajectory/signature between 1992 and 2008. This trend is different from that of cluster B over the period 2000-2008 period, but with a clear divergence for the last decade involving an erosive trend for cluster G and an accretive trend for cluster F. Erosion and accretion can be contemporaneous as can be accretion and stability, independently of the antecedent trend. These behavioural patterns show sometimes spectacular reversals (clusters A, B or F). All of these trends highlight the complexity of shoreline changes over the long term and on a regional scale. Even though shoreline movements close to an inlet are generally greater than those measured a few kilometres away, the ebb delta survey stations do not belong to a unique cluster (Fig. 6), and the survey locations belonging to same clusters appear spatially scattered.

Figure 6

4.2 Contemporary sea-level rise

The tide gauge in Saint-Malo (Fig. 1) shows a sea-level rise that has amounted to 2.04 mm/y ±0.68 mm/y between 1993 and 2018. This rise is characterised by strong inter-annual variability (Fig. 7). On Jersey Island (Fig. 1), 30 kilometres offshore of the study area, the relative sea-level rise between 1992 and 2016 from the PSMSL database has amounted to about 2.58 mm/y. The estimated absolute mean sea-level rise in Saint-Malo calculated from the synthesis carried out by Dodet et al. (2019) would be 1.41 mm/y. No land movement measurements are available from Jersey Island to enable calculation of an absolute mean sea-level rise (Prime, 2018).

Figure 7

4.3 Storms and wave activity during spring high tides

In additional to a historical perspective that summarises past multi-decadal storminess and the observed effects, the relationships between wave energy flux variations and shoreline changes were investigated over the time period of available HOMERE data. The number of events occasions coupling water levels higher than the MSWL with wave heights yields qualitative information on the wave climate in the study area. These data were previously normalised to enable comparison with the normalised data on shoreline changes. The latter were reduced to the 1994-2010 period, and we take into account only the data acquired at a seasonal timescale at a quasi-regular time step. As expected from a historical storminess perspective, shoreline retreat is observed during storms coinciding with spring tides (Tab. 2), even though beach parameters such as slope, sediment size and especially elevation prior to the storm are also relevant. Figure 2 shows the locations of the 8 HOMERE model points used to characterise the wave data and further analyse the wave spatial variability.

Table 2

Figures 8 shows the spatial and temporal variability of the number of events combining significant wave heights larger than 1 m and high-tide water levels exceeding the mean spring high-tide level. The event number change for each location is globally well correlated over the period 1994-2016 (HOMERE data availability). For each year, a clear decrease of this event number is observed from point HOMERE-7, close to Cape Carteret, to point HOMERE-14, close to Granville. This north-south diminishing gradient confirms the findings of Levoy et al. (2000) regarding a southward decrease in wave heights along the western part of the Cotentin Peninsula. The second result concerns the change trends of the event number for each location. Three periods are observed: the first, between 1994 and 2003, shows, for each location from north to south, a decreasing trend of the number of events (Fig. 8). Between 2004 and 2010, the number of events diminishes compared to the previous period, and the situation is globally stable. Finally, between 2011 and 2016, the trend is positive, showing an overall increase in the number of events despite an inter-annual variability that also concerns the previous periods.

Figure 8

This approach based on the analysis of the event number using HOMERE data is completed with wave data measured in the central part of the study area (Fig. 2) up to 2019, end of the study period. When the tidal level exceeds the MSWL, wave heights between 2 and 2.5 m are observed 9 times between 2014 and 2019, and only two times before, and wave heights between 2.5 and 3 m and > 3 m only in 2017 and 2018 (Storm Eleonor), respectively, but not before. Therefore, these results show clearly recent reinforced wave activity, not observed before, with extreme events that are a combination of strong waves and high water levels.

Wave heights from the HOMERE database can be used to calculate wave energy based on the van Rijn formula (van Rijn, 1990) and the methodology proposed in Robin et al. (2007). Only water levels > MSWL were included. Due to the seasonal nature of the wave climate, the calculation was carried out only for the winter months, between December and March. Figure 9 shows the mean curve of the winter energy flux obtained from the eight HOMERE locations. The trend previously described concerning stormy event numbers is logically also observed (Figs. 8, 9) with several multi-annual periods: decreasing wave energy between winter 1994/1995 and winter 1996/1997, then a positive change up to 1999/2000 and 2000/2001 winters followed, between the 2003/2004 and 2010/2011 winters by low wave energy, and thereafter a clear energy reinforcement. The evolution of the mean wave energy flux along the west coast of the Cotentin Peninsula during high water levels in the winter months between 1994 and 2016 (Fig. 9) offers, thus, an interesting signature of wave climate change, even though the database does not cover the entire study period.

Figure 9

The North Atlantic Oscillation (NAO) is well known to affect the wave climate in Europe. Castelle et al. (2017, 2018b) propose an optimized climate index they named Western Europe Pressure Anomaly (WEPA) that appears to be better adapted to the coast of Western Europe from Portugal to the UK than the NAO. Given the location of the Cotentin coast within this domain, we have applied the NAO and the WEPA indices to an analysis of the relationship, to

a first approach, between wave activity and large-scale oceanic and atmospheric variability. Figure 10 shows the NAO index for the winter months (December to March) and the WEPA index between 1994 and 2016. Both indices exhibit marked inter-annual variability.

Figure 10

These climatic indices are correlated with the mean energy flux of winter wave heights during spring tides (> MSWL) in the study area calculated from the HOMERE database (Fig. 11). The results highlight a good relationship between the annual winter wave energy and the WEPA index, better than that with the NAO index as indicated by the values of the correlation coefficients, respectively 0.69 and 0.12 (Fig. 11A and B). Wave activity along the west Cotentin coast can clearly be linked to the variability of atmospheric behaviour, probably due to the strong relationship between winds and the local wave regime.

Figure 11

5 Discussion

5.1 Shoreline changes

Shoreline changes along the west Cotentin coast have been analysed over a 27-year span of field surveys that have provided dimensional and normalised shoreline position changes from measurements three times a year during the first 16 years, and about once a year over the last decade. No filtering or smoothing procedures have been applied in order to conserve the effects of seasonal changes, major storms, sea level, or man-made structures over the multi-annual to multi-decadal trends. First at all, this dataset is unique in terms of its large spatial scale and its duration. Moreover, its seasonal time resolution, with about 60 surveys in May 2019 for 95% of the survey locations, is rare. While the mean spatial resolution is a little bit larger than that recommended by Hayden et al. (1979), the results obtained regarding temporal shoreline changes are useful to investigate the link between shoreline mobility and the driving factors.

The results show first complex shoreline behaviour both spatially and temporally, as often observed at a meso-scale by various authors, whatever the dataset used. Along the Cotentin coast, which is exclusively sandy, 51.5% of shoreline survey locations exhibit net retreat and 48.5% net advance, but the absolute values of the annual mean rates of eroding survey locations are greater by a factor 2, even sometimes 3, than for locations showing an accretive behaviour. These results are different from those of Bird (1985), but quite similar to those updated by Luijendijk et al. (2018) on a global scale when a threshold of 0.5 m/y is considered.

The normalised dataset and the cluster analysis used here to highlight the importance of temporal changes at the expense of their amplitude (e.g., Burningham and French, 2017; Burningham and Fernandez-Nunez, 2020) reveals complex behaviour that is rarely described in the literature due often to the lack of data with a high temporal resolution. Nine main clusters presenting each a specific Shoreline Temporal Change Signature (STCS) have been identified. These results highlight the non-linearity of the temporal behaviour at a timescale of almost three decades, confirming the findings of Pye and Blott (2008) for a macrotidal coast, while being slightly different from those of Guillen et al. (1999) for the Dutch coast (zones II and III in particular) with much lower tidal ranges. In fact, in Normandy, different trends,

sometimes involving reversals, are observed, mainly at multi-annual and sub-decadal timescales. This cluster analysis also reveals patterns different from those identified by Burningham and French (2017) on the meso-tidal Suffolk coast (UK) where 90% of the shoreline shows small-scale shifts with no significant trend or cyclicity between 1990 and 2015. However, the tidal range difference aside, the Suffolk coast is characterised by soft-rock cliffs punctuated by sand and gravel barriers and estuaries, and thus differs from the sandy and relatively homogeneous west Cotentin coast. In the latter, the proportion of shoreline stations classified in each cluster appears fairly balanced, between 5 and 16%, underlining the diversity of shoreline temporal behaviour. The relatively balanced net erosion and accretion in terms of location number suggests that the increased external forcing over the last decades (sea-level rise, meteo-ocean conditions) is strongly modulated by local controls that counteract the influence of wave change coupled with high tidal levels (Cazenave and Le Cozannet, 2014). The different STCS defined for each cluster suggest a large possibility of factors acting differently, spatially at a local and regional scale and temporally over variable durations. This temporal and spatial variability of shoreline behaviour brings out the multitude and, no doubt, complexity of factors acting on shoreline mobility at this nearly three-decade timescale and over a relatively large spatial scale, with dominant behavioural patterns, but also numerous local specificities. This complexity implies, thus, to a first approach, the exclusion of a regional and homogeneous effect. The main driving factors are conceptually summarised in Fig. 12 and their respective weights in the study area are discussed below. In addition to the two main factors that are the focus of this study – namely sea-level rise and storms and their impacts, a number of other less quantifiable factors have also modulated shoreline mobility. These include beach-dune morphometric characteristics that have not been investigated here, sediment availability and the influence of tidal inlets, and the perturbing influence of engineering structures.

Figure 12

5.2 Impact of sea-level rise, mean annual sea-level variability and multi-decadal tidal cycles on shoreline behaviour

Understanding shoreline response to sea-level rise is one of the major challenges in the coming decades (Cazenave and Le Cozannet, 2014; Vousdoukas et al., 2020; Cooper et al., 2020). Some authors (Leatherman et al., 2000; Zhang et al., 2004; Vousdoukas et al., 2020) have identified a good agreement between sea-level rise and average long-term shoreline retreat. These approaches are criticised for the choice of the study sites or for the use only of the Bruun rule (Cooper and Pilkey, 2004; Cooper et al., 2020) with its well-known limitations. The relationship between shoreline behaviour in the nine clusters identified as representative of the multi-decadal mobility patterns on the West Cotentin coast and mean sea-level variations can be considered at two temporal scales: the long-term, involving a rise of +2 mm/y at Saint-Malo, and a shorter-term with interannual fluctuations (Fig. 7) regressing sea level rise against shoreline change shows that no significant correlation, whatever the sea-level timescale, with R^2 values close to zero (Fig. 13).

Figure 13

No cluster shows a continuous nearly linear or linear trend in shoreline evolution typically induced by relative sea-level change (Stive et al., 2002) during the almost three decades covered by the study. This suggests that regional multi-decadal sea-level rise has not been

important in explaining shoreline mobility on the Normandy coast. The recorded rise of a few cm in 27 years is relatively small in the megatidal setting of this coast. The potential impact of sea-level rise and its interannual fluctuations is embedded in, or counter-balanced by other influencing factors, including sediment budget within individual cells, as has also been reported on the west coast of the UK (Pye and Blott, 2008), and as reported for various other global sites by Cooper et al. (2020). The shoreline mobility of the west Cotentin coast seems to be strongly modulated by driving factors that are less stable temporally and more active than mean sea-level rise.

The high tidal levels corresponding to the maximum elevations of the long-term tidal cycle in 1997 and 2015 (i.e. the 18.6 y lunar nodal tidal cycle; Gratiot et al., 2008; Levoy et al., 2017), allow high levels of wave attack, especially on coasts with large tidal ranges (Pye and Blott, 2008). Along the west Cotentin coast, this factor probably explains in part the number of erosive storm events during high tides exceeding the mean spring tide levels in winter 2013-2014, which was close to the 2015 peak in the lunar nodal tidal cycle. However, the observed shoreline changes around 1996/1997, when shoreline advance prevailed, are not coherent with the 1997 peak in the lunar nodal tidal cycle, thus suggesting that this factor alone cannot be responsible for extreme tides that induced shoreline retreat (Pye and Blott, 2008). It has also been suggested that the nodal tidal cycle influences regional mean sea level (Baart et al., 2012), but data on mean sea level for Saint-Malo over the period 1995-2019 showed a low value in 1997 (Fig. 7), a year corresponding to the peak of the high limb of the 18.6 y lunar nodal cycle. Such peaks can be countered in tidal records by meteorological activity, notably atmospheric pressure and wind speed and direction (Gerkema and Duran-Matute, 2017).

5.3 Trends in wave energy and storms and theirs impacts

Due to the large variability in shoreline mobility underlined by the cluster analysis, the links with wave climate appear contrasted and variable (Fig. 14). For the 1994-2010 period, the best correlations were obtained for clusters B and G, with R^2 up to 0.5 (significant at the 95% confidence level) during a significant time period up to 2004 (about ten years). After this, the coefficient decreases. Clusters A and E show moderate correlations of up to 0.3 before 2003 (significant at the 90% confidence level), but which also decrease afterwards. However, whereas for clusters B and G, erosion is somewhat correlated with increasing wave energy, inversely, for clusters A and E, increasing and decreasing wave energy correspond respectively to shoreline advance and shoreline retreat. It seems interesting to mention that the survey locations of clusters A and E are mainly within reach of the influence of an ebb delta or updrift of transversal beach structures where sediment availability is relatively high. For the other clusters C, D, F, H and I, the correlation coefficients are very low, underlining the importance of other driving factors of shoreline mobility. In this case, the influence of wave energy forcing during high water levels can be moderated or annulled by beach and dune foot morphometry characteristics as discussed below.

Figure 14

Over the last decade, the mean wave energy flux calculated from HOMERE data (2010/2011 winter - 2015/2016 winter) shows an increasing trend, the prevalence of which is confirmed by field wave measurements up to 2019. The 2013-2014 winter is considered as the most energetic along much of the Atlantic coast of Europe since at least 1948 (Masselink et al., 2016), and 2017-2019 wave measurements show also a high level of wave activity along the

west Cotentin coast. The reinforced wave activity during spring tides over this last decade appears linked to some patterns of shoreline mobility in the study area, and three clusters, i.e., E, G and I, show continuous shoreline retreat. A link exists, thus, between wave energy and shoreline change, but its expression is variable, depending on the period under consideration. Clusters E, G, and I concern only 37.5% of the survey locations.

The good correlation between wave energy and the WEPA index (Fig. 11B) enables an extrapolation of wave energy prior to and after the HOMERE period. Figure 15 shows the very large fluctuations of winter wave energy in the study area, especially since the beginning of the 1990s, confirming the recent increasing variability of wave activity reported by Castelle et al. (2018b). This correlation suggests also the high level of wave energy between the mid-1970s and the end of 1980s, akin to that observed since 2010, deduced from the mean trend (red dotted line). This active period is well known with successive severe storms during spring tides that resulted in important shoreline erosion and flooding in the study area (Tab. 2) and more widely along the northwest coast of France. It shows the pertinence of the use of climatic indexes to forecast future wave activity periods and potential induced shoreline changes. These results confirm also the findings of Pye and Blott (2008) regarding the effects of extreme high tides combined with storm wave activity on temporal shoreline variations. Whereas the temporal shoreline behavioural links to oceanographic forcing appear as a large-scale influence (Hapke et al., 2016), observed from north to south of the western Cotentin Peninsula, other patterns are not explained by this forcing.

Figure 15

From a physical point of view, waves need to coincide with a water level that is high enough for runup to attain, and eventually initiate erosion of the dune foot. The observations reported in Tab. 2 show that this minimum level is close to the mean theoretical high spring tide level. It is also important to consider storm surge levels that further raise the level of action of incident waves at high tide. A storm surge attained, for instance, +1.6 m at Granville on 16 October 1987 (Levoy, 1994). These storm surges have also exhibited marked regional variability over the time span of our study (Turki et al., 2020). In addition to climatic variability, these levels are further influenced by strong interannual variability under the joint impact of mean sea-level fluctuation and the 18.6-year nodal tidal cycle (Haigh et al, 2010).

At Granville and Carteret, respectively in the southern and northern sectors of the study site, the theoretical spring high water level can fluctuate over a range of 1.59 m and 1.17 m, respectively, between mean and exceptional high spring tides (SHOM, 2022). This vertical range of the tidal excursion over a period of 27 years is much larger than the regional sea-level rise and its interannual fluctuations (Fig. 7). The effect of sea-level rise can also be largely superseded by that of storm surge levels that exceptionally attained, for instance, 1.6 m at Granville during the storm of 16 October 1987 (Levoy, 1994). Although high wave runup levels during high spring tides are reported for beaches with large tidal ranges (Cariolet and Suanez, 2013), these do not necessarily lead to dune-foot erosion on the Normandy coast. The correlation between high waves during spring high tides and shoreline mobility is not always good (Fig. 14) for certain clusters and certain periods of time. In addition to wave and tidal conditions, shoreline mobility also depends on beach, dune and shoreface morphology (Guillen et al., 1999; Saye et al., 2005; Cohn et al., 2019), and beach elevation, sediment volume and width (Richter et al., 2013; Crapoulet et al., 2016). Fluctuations in beach elevation in the study area can attain up to 2.8 m (Levoy et al., 2000), and can thus significantly modulate the duration of wave influence and energy levels at the dune foot

(Masselink et al., 2022). These fluctuations in beach elevation depend in part on sediment availability but are also influenced by tidal inlets and engineering structures.

5.4 Sediment availability and inlet influence

Shoreline change responds to other driving factors acting together with water levels and wave activity. Sediment transport, especially alongshore, as observed along the west Cotentin coast, modulates, at a decadal timescale, beach elevation, especially of the upper foreshore on tidal sandy beaches. Moreover, sand availability is a key point to consider regarding beach and shoreline changes. On the west Cotentin coast, the lower foreshore is often bedrock, partially always below the lowest water level. This particularity contributes to reducing potential onshore sand transfers from the shoreface, but also loss of sand from beaches during storms, and these conditions are favourable to the stability of beaches and shoreline positions. A continuous sand cover extending to the shoreface is generally observed in front of the large ebb deltas. The others are too small to be connected to the shoreface. The magnitude and alongshore directions of the tidal currents on the shoreface, even in front of the main ebb deltas, can also reduce cross-shore sand transfers between the shoreface and the beaches. The beaches of the west Cotentin coast seem rather impervious to large cross-shore sand movements and their mobility is mainly due to longshore transport induced by waves on the upper and mid-foreshore, and secondarily by tidal currents on the lower foreshore (Levoy et al., 2000, 2001), a pattern quite different from that observed on many wave-influenced sandy shorefaces (Anthony and Aagaard, 2020).

However, sediment supply shows a regional specificity in the central part of the western basin of the English Channel where a particularly high proportion of bioclastic sediment is observed, ranging up to 80% (Larsonneur et al., 1982). This rate is comprised between 30 and 40% on the upper foreshore along the west coast of the Cotentin Peninsula (Lafond, 1986). Unfortunately, the annual amount of this production is unknown, but could potentially be considered as an unlimited source of sand for coastal dunes, as in Australia (Anthony and Aagaard, 2020). This active carbonate supply may contribute also to explain the relative equilibrium between the total lengths of shoreline subject to erosion and accretion in the study area.

The largest shoreline changes along the west coast of the Cotentin Peninsula are observed close to the inlets, thus confirming, for the megatidal environment of Normandy, similar findings for coasts with much lower tidal ranges (Fitzgerald, 1984; 1988; Castelle et al., 2018a, Konlechner et al., 2020; Nmiss et al., 2022). As zones of longshore sand convergences, well-connected to shoreface sediment stocks, the main tidal inlets and their ebb deltas are the intertidal areas showing the largest topographic changes. The onshore migration of swash bars towards spit ends and their attachment under stormy conditions (Robin and Levoy, 2007; Robin et al., 2007; Robin et al., 2009a, 2009b) are one of the main causes responsible for large shoreline changes (Fitzgerald, 1984; 1988; Konlechner et al., 2020). Accretive shorelines can be observed over the last decade, despite the reinforced wave activity, due to onshore swash bar migration, as for survey stations of clusters A and B. But downdrift of the attachment location of a swash bar to the upper foreshore, intense recent erosion can lead to large breaches, as on Pointe d'Agon (Robin et al., 2020) and Pointe du Banc (Fruergaard et al., 2020). This process can lead to the mobilisation of significant volumes of sand, and confirms, for the latter spit, a by-passing process associated with a strong reverse shoreline behaviour on the downdrift side of the inlet (survey location SW33,

cluster A). Often cited as an uncommon event (Fitzgerald, 1988), observed during extreme storms (Sánchez-Arcilla and Jiménez, 1994; Chaumillon et al., 2014; Zăinescu et al., 2019), breaching has occurred many times on the updrift sides of spits along the west Cotentin coast in the course of the 27 years of the study period. Strong shoreline retreat has also been observed on the downdrift side of an inlet due to the migration of the main tidal channel meander towards the shoreline induced by the growth of the dominant spit on the updrift side (Chaumillon et al., 2014). This also led to large breaches in the past (Havre de Regnéville; Levoy, 1985, 1988), but also recently along the Lingreville inlet spit. While these important erosional processes contribute to shoreline retreat at a short timescale, the residual long-term longshore transport favours the accretion of spit shorelines. An example of this accretion was observed at Pointe d'Agon where a residual sand deposition of about 244,000 m^3 over a period of 10 years occurred at the tip of the spit and led to the construction of a new hook (Robin et al., 2020). These sand movements and the possible sediment recirculation generated by tidal currents over the ebb delta surfaces (Levoy et al., 2013; Montreuil et al., 2014) are the main driver of shoreline mobility along several kilometres on each side of the inlets, thus confirming findings from other areas with lower tidal ranges (Fitzgerald, 1984; Fenster and Dolan, 1996).

Beyond the impacts of local inlet dynamics on shoreline mobility, antecedent regional hydrodynamic conditions, especially under conditions of relative stability at a decadal timescale, are important in attempting to explain morphological changes along sandy coasts (Thomas et al., 2016). As indicated previously, the winters from the mid-1970s to 1990, observed in the course of the decade prior to the beginning of the shoreline surveys reported here, were generally very energetic (Fig. 15), and storms deprived already sand-deficient beaches of sediment, as attested by the steep morphology of upper foreshores and the numerous breaches and washover fans near eroded dune fronts (Tab. 2). This degraded shoreline at the beginning of the 1990s may largely explain the dominant shoreline constructive or stability phase often observed in the course of the first 15 years of monitoring which coincided with a decreasing trend in mean wave energy during spring tides (Fig. 9), favouring, first, beach recovery, and then shoreline advance. These results suggest that, at a multi-decadal timescale, wave action during high tides exceeding the mean spring tides can correlate well with sediment supply and shoreline changes.

5.5 Impacts of coastal engineering structures and beach management

Shoreline management (e.g. defence structures, beach or dune-front nourishments, jetties, port structures) is a driving factor of beach and shoreline changes, as several authors have shown (e.g. Bruun, 1995; Slott et al., 2010; Cooper and Pilkey, 2012; Pranzini, 2013; Anthony et al., 2019). On the west Cotentin coast, some stretches of shoreline exhibit a high density of anthropogenic interventions (Fig. 3), while others appear to be more natural, without visible human influences and sometimes far from an inlet. This variability appears useful in discriminating the respective influences of factors controlling shoreline changes, but also in explaining mean rates of change, as a strong correlation sometimes exists between the level of development and regional rates of change (Hapke et al., 2013).

Considering especially the overarching importance of longshore sediment transport on the west Cotentin coast, jetties built across shore to fix a main channel in an inlet entrance, groyne fields, and even concrete beach accesses, have a negative effect on shoreline stability. This is observed for survey stations of cluster H during the first two decades, with breaches

close to Regnéville and Lessay inlets. The sediment transported alongshore is intercepted by these structures, resulting in a hotspot of sediment deficit on the downdrift side and intense shoreline advance updrift. The effect of groyne fields depends on their efficiency in stopping or reducing longshore transport (e.g., Uda, 2010; Ndour et al., 2018). Positive effects of this type of structure are, however, observed, as over the last decade for clusters B and F. This tends to counteract the effect of recently reinforced wave activity and promotes stability or net shoreline accretion, as on the updrift side of engineered inlets on the US east coast (Hapke et al., 2013). These consequences are similar to those mentioned along the coasts of Africa following the construction of several seaports (Elmoustapha et al., 2007; Giardino et al., 2018; Anthony et al., 2019), with shoreline advance along the updrift side and erosion along the downdrift side of the port breakwaters. As all these cross-shore structures are relatively permanent (>10 years), and their impacts on shoreline change may also persist for long periods of time (Hapke et al., 2013). However, spatially, they are relatively local features.

Beach nourishments on a regular basis can be positive in the long term, but not always at the location of the initial recharge. In Barneville-Carteret, a beach nourishment of about 130,000 m^3 of sand was carried out to stop erosion of the upper foreshore in front of an armoured seawall and downdrift shoreline retreat. This sand mass has moved alongshore slowly, leading to accretion of the shoreline downdrift of the nourishment over the last two decades. This contributes to explaining, in like fashion of the impacts on the updrift side of cross-shore structures, the shoreline mobility of cluster F. Some sites combine multiple driving factors controlled by human interventions that induce active erosion or accretion.

6 Conclusions

Shoreline changes on the west Cotentin coast Normandy, France, show, at a multi-decadal scale, as along many sandy coasts in the world, a large space and time variability. The maximum retreat measured over a 27-year period of fine-tuned monitoring reaches 220 m and advances of up to 110 m were recorded. Accretive and erosive locations along this straight sandy coast appear well balanced, respectively 51.5 and 48.5%, even though yearly largest accretion rates are lower than erosive ones by a factor 2, and even more for some hotspots in particular near inlets. An original dendrogram summary of these mobility patterns suggests spatially variable time-changing trends, especially reversals. These results suggest the interplay of several driving factors of shoreline change acting from a multi-annual to a multi-decadal scale.

The diverse shoreline mobility patterns highlighted by nine clusters suggest that neither mean regional sea-level rise nor interannual sea-level variability have played an important role over the multi-decadal time frame of the study and the megatidal context. An inventory of the main historical storms that struck the west Cotentin coast highlighted the role of very high tidal levels (spring tides) combined with wave action to explain shoreline retreat and associated damages (breaching, flooding and damages to coastal protection works). However, the storm surges during these historical events were moderate (< 0.65 m), thus underlining, rather, the importance of tidal range during these spring tide conditions. In view of these results, the analysis of the wave data focussed exclusively on water levels exceeding mean spring tide water levels at high tide. However, the shoreline behaviours that match with this wave energy/tidal level picture represent at best only 37.5% of the survey locations, and this only over the last decade. The diversity of shoreline mobility suggests, thus, other influences, notably inlet dynamics and human-made structures for coastal protection, beach access and navigation purposes, which generally modify beach morphology and elevation, and the

overall local beach sediment budget, with consequences on high-tide wave impact on shoreline mobility. An analysis of beach elevation changes and their temporal mobility as a proxy for sand supply over the last three decades, but also the link between the shoreface and the foreshore, given the importance of offshore carbonate production in the sediment budget of beaches and dunes in the study area, may help in clarifying these effects.

Overall, the potentially variable shoreline mobility highlighted by the relatively good-resolution Cotentin coast database prompts caution in any attempt to predict future shoreline locations, a commonly pressing demand from coastal management authorities concerned with climate change and sea-level rise. While the influence of sea level rise within the 27-year time frame of the present study has been shown to be limited, this factor will be of increasing concerned in the future, with important, potentially negative, implications for shoreline mobility on the low sandy sectors of the Normandy coast.

Acknowledgements

The monitoring of coastal change along the western coast of Cotentin peninsula initiated in 1991 constitutes a long story of contacts with many people, teams and organisms. Firstly, this study was supported mainly by the Conseil Départemental de la Manche since 1991, with the help of the Conseil Régional of Normandy during some years. This study was also supported in part by CNRS-INSU and four French regions: Basse-Normandie, Haute-Normandie, Picardie and Nord-Pas-de-Calais during the LiDAR CLAREC project (2008-2014). The authors would like to thank the successive field teams during these three decades of surveys, in particular driven by Olivier Labomme, Patrice Bretel, Emmanuel de Saint-Léger, Hervé Bizien and Yoann Bonte, as Professor Claude Larsonneur who enabled the setting-up and supervision of the project in its initial stage. We would also like to thank Hélène Rousset for her contribution to the processing of the data. We thank also the CLAREC and CIRCLE teams for conducting the LiDAR surveys, especially Patrice Bretel who prepared the data and the CREC technical team for preparing some specific equipment, especially Jean-Paul Lehodey. Thanks also to Guillaume Izabel, CREC, for its implication in this project, beyond the scope of this paper (webmaster of the website) and for preparing the first version of the heatmap. Thanks also to Bruno Castelle from CNRS/University of Bordeaux for providing WEPA index, to the ROLNP for 2016 LiDAR Data and to the DDTM of Département de la Manche for information about coastal structures. We thank the two anonymous reviewers and the Editor-in-Chief for the constructive revision suggestions.

7 References

Anthony, E.J., 2009. Shore Processes and their Palaeoenvironmental Applications. Developments in Marine Geology Volume 4. Elsevier Science, Amsterdam, 519 pp (see Chapter 10 in particular).

Anthony, E.J., 2013. Storms, shoreface morphodynamics, sand supply, and the accretion and erosion of coastal dune barriers in the southern North Sea. Geomorphology 199, 8-21. https://doi.org/10.1016/j.geomorph.2012.06.007.

Anthony, E.J., Almar, R., Besset, M., Reyns, J., Laibi, R., Ranasinghe, R., Abessolo Ondoa, G., Vacchi, M., 2019. Response of the Bight of Benin (Gulf of Guinea, West Africa) coastline to anthropogenic and natural forcing, Part 2: Sources and patterns of sediment supply,

788 sediment cells, and recent shoreline variations. Cont. Shelf Res. 173, 93-103.
789 https://doi.org/10.1016/j.csr.2015.09.020.

790 Anthony, E.J., Aagaard, T., 2020. The lower shoreface: Morphodynamics and sediment
791 connectivity with the upper shoreface and beach. Earth-Science Reviews 210(C3), 103334.
792 https://doi.org/10.1016/j.earscirev.2020.103334.

793 Baart, F., van Gelder, P.H.A.J.M., de Ronde, J., van Koningsveld, M., Wouters, B. 2012. The
794 effect of the 18.6-year lunar nodal cycle on regional sea-level rise estimates. J. Coast. Res. 28:
795 511-516. https://doi.org/10.2112/JCOASTRES-D-11-00169.1.

796 Besset, M., Anthony, E.J., Bouchette, F., 2019. Multi-decadal variations in delta shorelines
797 and their relationship to river sediment supply: An assessment and review. Earth-Science
798 Reviews, 193-199-219. https://doi.org/10.1016/j.earscirev.2019.04.018.

799 Bird, E.C.F., 1985. Coastline changes: A Global Review. Wiley, Chichester.

800 Boak, E., Turner, I., 2005. Shoreline Definition and Detection: A Review. J. Coastal Research
801 21, 688-703. http://dx.doi.org/10.2112/03-0071.1.

802 Boudière, E., Maisondieu, C., Ardhuin, F.,Accensi, M.,Pineau-Guillou, L., Lepesqueur, J.,
803 2013. A suitable metocean hindcast database for the design of Marine energy converters.
804 International Journal of Marine Energy 3-4, e40-e52.
805 http://dx.doi.org/10.1016/j.ijome.2013.11.010.

806 Bruun, P., 1995. The development of downdrift erosion. J. Coast. Res. 11, 1242-1257.
807 https://www.jstor.org/stable/4298427.

808 Burningham, H., French, J., 2017. Understanding coastal change using shoreline trend
809 analysis supported by cluster-based segmentation. Geomorphology 282, 131-149.
810 https://doi.org/10.1016/j.geomorph.2016.12.029.

811 Burningham, H., Fernandez-Nunez, M., 2020. Shoreline change analysis, in: Jackson, D.W.T.
812 et al. Sandy beach morphodynamics, pp. 439-460. http://dx.doi.org/10.1016/B978-0-08-
813 102927-5.00019-9.

814 Cariolet, J.M., Suanez, S., 2013. Runup estimations on a macrotidal sandy beach. Coast. Eng.
815 2013, 74, 11-18. https://doi.org/10.1016/j.coastaleng.2012.11.008.

816 Castelle, B., Dodet, G., Masselink, G., Scott, T., 2017. A new climate index controlling winter
817 wave activity along the Atlantic coast of Europe: The West Europe Pressure Anomaly.
818 Geophysical Research Letters 44, 1384-1392. https://doi.org/10.1002/2016GL072379.

819 Castelle, B., Guillot, B., Marieu, V., Chaumillon, E., Hanquiez, V., Bujan, S., Poppeschi, C.,
820 2018a. Spatial and temporal patterns of shoreline change of a 280-km high-energy disrupted
821 sandy coast from 1950 to 2014: SW France. Estuar. Coast. Shelf Sci. 200, 212-223.
822 https://doi.org/10.1016/j.ecss.2017.11.005.

823 Castelle, B., Dodet, G., Masselink, G., Scott, T., 2018 b. Increased winter-mean wave height,
824 variability, and periodicity in the northeast Atlantic over 1949-2017. Geophysical Research
825 Letters 45. https://doi.org/10.1002/2017GL076884

826 Cazenave, A, Le Cozannet, G., 2014. Sea level rise and its coastal impacts. Earth's Future 2,
827 15-34. https://doi.org/10.1002/2013EF000188.

828 Chaumillon, E., Ozenne, F., Bertin, X., Long, N., Ganthy, F., 2014. Control of wave climate
829 and meander dynamics on spit breaching and inlet migration. Journal of Coastal Research 70,
830 109-114. https://doi.org/10.2112/SI70-019.1.

831 Chaverot, S., Héquette, A., Cohen, O., 2008. Changes in storminess and shoreline evolution
832 along the northern coast of France during the second half of the 20 century. Z. Geomorphol.
833 52 Supplementary Issues 3, 1-20. https://doi.org/10.1127/0372-8854/2008/0052S3-0001.

834 Cohn, N., Ruggiero, P., García-Medina, G., Anderson, D., Serafin, K.A., Biel, R., 2019.
835 Environmental and morphologic controls on wave-induced dune response. Geomorphology,
836 329, 108-128. https://doi.org/10.1016/j.geomorph.2018.12.023.

837 Cooper, J.A.G., Pilkey, O.H., 2004. Sea-level rise and shoreline retreat: time to abandon the
838 Bruun Rule. Global and Planetary Change 43 157-171.
839 https://doi.org/10.1016/j.gloplacha.2004.07.001.

840 Cooper, J.A.G., Masselink, G., Coco, G., Short, A.D., Castelle, B., Rogers, K., Anthony, E.,
841 Green, A.N., Kelley, J.T., Pilkey, O.H., Jackson, D.W.T., 2020. Sandy beaches can survive
842 sea-level rise. Nat. Clim. Chang. 10 (11), 993-995. https://doi.org/10.1038/s41558-020-
843 00934-2.

844 Crapoulet, A., Héquette, A., Marin, D., Levoy, F., Bretel, P., 2017. Variations in the response
845 of the dune coast of northern France to major storms as a function of available beach sediment
846 volume. Earth Surface Processes and Landforms, 42 (11), 1603-1622.
847 https://doi.org/10.1002/esp.4098.

848 Crowell, M., Douglas, B.C., Leatherman, S.P., 1997. On forecasting future U.S. shoreline
849 positions: a test of algorithms. Journal of Coastal Research 13(4), 1245-1255.
850 https://www.jstor.org/stable/4298734.

851 Dean, R.G., Houston, J.R., 2016. Determining shoreline response to sea level rise. Coastal
852 Engineering 114, 1-8. http://dx.doi.org/10.1016/j.coastaleng.2016.03.009.

853 Del Río, L., Gracia, F.J, Benavente, J., 2013. Shoreline change patterns in sandy coasts. A
854 case study in SW Spain. Geomorphology 196, 252- 266.
855 http://dx.doi.org/10.1016/j.geomorph.2012.07.027.

856 Dodet, G., Bertin, X., Bouchette, F., Gravelle, M., Testut, L., Wöppelmann, G., 2019.
857 Characterization of sea-level variations along the metropolitan coasts of France: Waves, tides,
858 storm surges and long-term changes. *In:* Castelle, B. and Chaumillon, E. (eds.), Coastal
859 Evolution under Climate Change along the Tropical Overseas and Temperate Metropolitan
860 France. Journal of Coastal Research, Special Issue No. 88, 10-24. Coconut Creek (Florida),
861 ISSN 0749-0208. https://dx.doi.org/10.2112/SI88-003.1.

862 Dolan, R., Fenster, M.S., Holme, S.J., 1991. Temporal analysis of shoreline recession and
863 accretion. Journal of Coastal Research, 7(3), 723-744. https://www.jstor.org/stable/4297888.

Elmoustapha, A.O., Levoy, F., Monfort, O., Koutitonsky, V., 2007. A Numerical Forecast of Shoreline Evolution after Harbour Construction in Nouakchott, Mauritania. Journal of Coastal Research, 23 (6), 1409-1417. http://dx.doi.org/10.2112/04-0423.1.

Fenster, M., Dolan, R., 1996. Assessing the impact of tidal inlets on adjacent barrier island shorelines. J. Coast. Res. 12, 294-310. https://www.jstor.org/stable/4298482.

Feser, F., Barcikowska, M., Krueger, O., Schenk, F., Weisse, R., Xia, L., 2015. Storminess over the North Atlantic and northwestern Europe-a review. Quarterly Journal of the Royal Meteorological Society 141(687), 350-382. https://doi.org/10.1002/qj.2364.

FitzGerald, DM., 1984. Interactions between the ebb-tidal delta and landward shoreline: Price Inlet, South Carolina. Journal of Sedimentary Petrology 54(4), 1303-1318. https://doi.org/10.1306/212F85C6-2B24-11D7-8648000102C1865D.

FitzGerald, D.M. 1988. Shoreline erosional-depositional processes associated with tidal inlets. In Aubrey D.G., Weishar L. (Eds), Lecture Notes on Coastal and Estuarine Studies *Vol. 29:* Hydrodynamics and Sediment Dynamics of Tidal Inlets. Springer-Verlag: New York, 186-224. http://dx.doi.org/10.1029/LN029p0186.

Fruergaard, M., Tessier, B., Poirier, C., Mouazé, D., Weill, P, Noël, S., 2020. Depositional controls on a hypertidal barrier-spit system architecture and evolution, Pointe du Banc spit, north-western France. Sedimentology 67, 502-533. https://dx.doi.org/10.1111/sed.12652.

Gallop, S.L., Kennedy, D.M., Loureiro, C., Naylor, L.A., Muñoz-Pérez, J.J., Jackson, D.W., Fellowes, T.E., 2020. Geologically controlled sandy beaches: their geomorphology, morphodynamics and classification. Science of the Total Environment 731, 1-14. https://doi.org/10.1016/j.scitotenv.2020.139123.

Gerkema, T., Duran-Matute, M., 2017. Interannual variability of mean sea level and its sensitivity to wind climate in an inter-tidal basin. Earth Syst. Dynam., 8, 1223-1235. https://doi.org/10.5194/esd-8-1223-2017.

Giardino, A., Schrijvershofa, R., Nederhoffa, C.M., de Vroega, H., Brièrea, C., Tonnona, P.K., Cairesa, S., Walstraa, D.J., Sosac, J., van Versevelda, W., Schellekensa, J., Sloffa, C.J., 2018. A quantitative assessment of human interventions and climate change on the West African sediment budget. Ocean Coast. Manag. 156, 249-265. https://doi.org/10.1016/j.ocecoaman.2017.11.008.

Guillen, J., Stive, M.J.F., Capobianco, M., 1999. Shoreline evolution of the Holland coast on a decadal scale. Earth Surf. Processes Landf. 24, 517- 536. https://doi.org/10.1002/(SICI)1096-9837(199906)24:6%3C517::AID-ESP974%3E3.0.CO;2-A.

Gratiot, N., Anthony, E.J., Gardel, A., Gaucherel, C., Proisy, C., Wells, J.T., 2008. Significant contribution of the 18.6 year tidal cycle to regional coastal changes. Nat. Geosci. 1(3), 169-172. https://dx.doi.org/10.1038/ngeo127.

Haigh, I., Nicholls, R., Wells, N., 2010. Assessing changes in extreme sea levels: Application to the English Channel, 1900-2006. Cont. Shelf Res., 30(9), 1042-1055. https://doi.org/10.1016/j.csr.2010.02.002.

Hapke, C.J., Lentz, E.E., Gayes, P.T., McCoy, C.A., Hehre, R.E., Schwab, W.C., Williams, S.J., 2010. A review of sediment budget imbalances along Fire Island, New York: can nearshore geologic framework and patterns of shoreline change explain the deficit? J. Coast. Res. 26, 510-522. https://doi.org/10.2112/08-1140.1.

Hapke, C.J., Kratzmann, M.G., Himmelstoss, E.A., 2013. Geomorphic and human influence on large-scale coastal change. Geomorphology 199, 160-170. http://dx.doi.org/10.1016/j.geomorph.2012.11.025.

Hapke, C.J., Plant, N.G., Henderson, R.E., Schwab, W.C., Nelson, T.R., 2016. Decoupling processes and scales of shoreline morphodynamics. Mar. Geol. 381, 42-53. https://doi.org/10.1016/j.margeo.2016.08.008.

Harley, M.D., Turner, I.L., Kinsela, M.A., Middleton J.H., Mumford, P.J., Splinter, K.D., Phillips, M.S., Simmons, J.A., Hanslow, D.J., Short, A.D., 2017. Extreme coastal erosion enhanced by anomalous extratropical storm wave direction. Sci. Rep. 7(1), 6033. https://doi.org/10.1038/s41598-017-05792-1.

Hayden, B., Dolan, R., Felder, W., 1979. Spatial and temporal analyses of shoreline variations. Coastal Engineering 2, 351-361. https://doi.org/10.1016/0378-3839(78)90031-5.

IPCC (Intergovernmental Panel on Climate Change), 2022. 6th Assessment Report. https://www.ipcc.ch/report/ar1/wg1/sea-level-rise/.

Konlechner, T.M., Kennedy, D.M., O'Grady, J.J., Leach, C., Ranasinghe, R., Carvalho, R.C., Luijendijk, A.P., McInnes, K.L., Ierodiaconou, D., 2020. Mapping spatial variability in shoreline change hotspots from satellite data; a case study in southeast Australia. Estuar. Coast. Shelf Sci. 246, 107018. https://doi.org/10.1016/j.ecss.2020.107018.

Kroon, A., Larson, M., Moller, I., Yokoki, H., Rozynski, G., Cox, J., Larroude, P., 2008. Statistical analysis of coastal morphological data sets over seasonal to decadal time scales. Coastal Engineering 55, 581-600. https://doi.org/10.1016/j.coastaleng.2007.11.006.

Lafond, L.R., 1986. La carte morphosédimentaire des zones intertidales du Golfe normand-breton au 1/25000 ème : Côte ouest du Cotentin et baie du Mont-Saint-Michel, 85 p.

Larsonneur, C., Bouysse, P., Auffret, J.P., 1982. The superficial sediments of the English Channel and its western approaches. Sedimentology *29*, 851-864. https://doi.org/10.1111/j.1365-3091.1982.tb00088.x.

Lazarus, E.D., Murray, A.B., 2007. Process signatures in regional patterns of shoreline change on annual to decadal time scales. Geophys. Res. Lett. 34(19), L19402. http://dx.doi.org/10.1029/2007GL031047.

Leatherman, S.P., Douglas, B.C., 2003. Sea level and coastal erosion require large-scale monitoring. Eos Transactions American Geophysical Union 84(2), 13-20. http://dx.doi.org/10.1029/2003EO020001.

940 Leatherman, S.P., Zhang, K., Douglas, B.C., 2000. Sea Level Rise Shown to Drive Coastal
941 Erosion. EOS Transactions 81(6), 55–57. https://doi.org/10.1029/00EO00034.

942 Le Cozannet, G., Garcin, M., Yates, M., Idier, D., Meyssignac, B., 2014.Approaches to
943 evaluate the recent impacts of sea-level rise on shoreline changes. Earth Sci. Rev. 138, 47-60.
944 https://doi.org/10.1016/j.earscirev.2014.08.005.

945 Le Cozannet, G., Bulteau, T., Castelle, B., Ranasinghe, R., Woppelmann, G., Rohmer, J.,
946 Bernon, N., Idier, D., Louisor, J., Salas-y-Melia, D., 2019. Quantifying uncertainties of sandy
947 shoreline change projections as sea level rises. Sci. Rep. 9(42).
948 https://doi.org/10.1038/s41598-018-37017-4.

949 Le Mauff, B., Juigner, M., Ba, A., Robin, M., Launeau, P., Fattal P. 2018. Coastal monitoring
950 solutions of the geomorphological response of beach-dune system using multi-temporal
951 LiDAR datasets (Vendée coast, France). Geomorphology 304, 121-140.
952 https://doi.org/10.1016/j.geomorph.2017.12.037.

953 Lerma, A.N., Ayache, B., Ulvoas, B., Paris, F., Bernon, N., Bulteau, T., Mallet, C., 2019.
954 Pluriannual beach-dune evolutions at regional scale: Erosion and recovery sequences analysis
955 along the aquitaine coast based on airborne LiDAR data. Cont. Shelf Res. 189, 103974.
956 https://dx.doi.org/10.1016/j.csr.2019.103974.

957 Levoy, F., 1985. Les risques littoraux en milieux littoraux sableux : côte ouest du Cotentin.
958 Université de Caen, CREGEPE. 292 p.

959 Levoy, F., 1988. Erosions et submersions sur les côtes du département de la Manche durant
960 l'hiver 1987-1988. Université de Caen, CREGEPE, Note n°1, 14-16.

961 Levoy F., 1994. Evolution et fonctionnement hydrosédimentaire des plages macrotidales :
962 L'exemple de la côte ouest du Cotentin. PhD thesis, Université de Caen. 423 p.

963 Levoy, F., Monfort, O., Rousset, H., 1994a. Sediment transport under wave-current
964 interaction on macrotidal beaches (Normandy, France). Proceedings Coastal Sediment' 94,
965 Barcelona, 727-741.

966 Levoy, F., Monfort, O., Rousset, H., Larsonneur, C., 1994b. Quantification of longshore
967 transport in the surf zone on macrotidal beaches: Fields experiments along the western coast
968 of Cotentin (Normandy, France). 24 th International Conference on Coastal Engineering,
969 Kobé, Japan. 2282-2296. http://dx.doi.org/10.1061/9780784400890.166.

970 Levoy, F., Anthony, E.J., Monfort, O., Larsonneur, C., 2000. The morphodynamics of
971 megatidal beaches in Normandy, France. Marine Geology 171, 39-59.
972 http://dx.doi.org/10.1016/S0025-3227(00)00110-9.

973 Levoy, F., Monfort, O., Larsonneur, C., 2001. Hydrodynamic variability on megatidal
974 beaches, Normandy, France. Continental Shelf Research 21, 563-586.
975 https://doi.org/10.1016/S0278-4343(00)00128-X.

976 Levoy, F., Anthony, E.J., Monfort, O., Robin, N., Bretel, P., 2013. Formation and migration
977 of transverse bars along a tidal sandy coast deduced from multi-temporal Lidar datasets. Mar.
978 Geol. 342, 39-52. http://dx.doi.org/10.1016/j.margeo.2013.06.007.

979 Levoy, F., Garestier, F., Froideval, L., Monfort, O., Poullain, E., 2016. Contribution of
980 airborne topographic LiDAR to the study of coastal systems. In Baghdadi N., Zribi M. (Eds),
981 Land Surface Remote Sensing in Urban and Coastal Areas, Elsevier: Amsterdam, 231-268.
982 https://dx.doi.org/10.1016/B978-1-78548-160-4.50006-6.

983 Levoy, F., Anthony, E.J., Dronkers, J., Monfort, O., Izabel, G., Larsonneur, C. 2017.
984 Influence of the 18.6-year lunar nodal tidal cycle on tidal flats: Mont-Saint-Michel Bay,
985 France. Marine Geology 387, 108-113. https://dx.doi.org/10.1016/j.margeo.2017.03.009.

986 Levoy, F., Anthony, E.J., Dronkers, J., Monfort, O., Montreuil, A.-L., 2019. Short-term to
987 decadal-scale sand flat morphodynamics and sediment balance of a megatidal bay: Insight
988 from multiple LiDAR datasets. In: Castelle, B., Chaumillon, E. (Eds.), Coastal Evolution
989 under Climate Change along the Tropical Overseas and Temperate Metropolitan France.
990 Journal of Coastal Research, Special Issue No. 88, 61-76. Coconut Creek (Florida), ISSN
991 0749-0208. https://doi.org/10.2112/SI88-006.1.

992 Luijendijk, A., Hagenaars, G., Ranasinghe, R., Baart, F., Donchyts, G., Aarninkhof, S., 2018.
993 The state of the world's beaches. Nat. Sci. Rep. 8, 6641. http://dx.doi.org/10.1038/s41598-
994 018-24630-6.

995 Masselink, G., Scott, T., Poate, T., Russell, P., Davidson, M., Conley, D., 2016. The extreme
996 2013/2014 winter storms: Hydrodynamic forcing and coastal response along the southwest
997 coast of England. Earth Surf. Process. Landf. 41, 378-391. https://doi.org/10.1002/esp.3836.

998 Masselink, G., Brooks, S., Poate, T., Stokes, C., Scott, T., 2022. Coastal dune dynamics in
999 embayed settings with sea-level rise - Examples from the exposed and macrotidal north coast
1000 of SW England. Marine Geology, 450, 106853.
1001 https://doi.org/10.1016/j.margeo.2022.106853.

1002 Mentaschi, L., Vousdoukas, M.I., Pekel, J.F., Voukouvalas, E., Feyen, L., 2018. Global long-
1003 term observations of coastal erosion and accretion. Sci. Rep. 8(1), 1-11.
1004 https://doi.org/10.1038/s41598-018-30904-w.

1005 Montaño, J., Coco, G., Antolínez, J.A.A., Beuzen, T., Bryan, K.R., Cagigal, L., Castelle, B.,
1006 Davidson, M.A., Goldstein, E.B., Ibaceta, R., Idier, D., Ludka, B.C., Masoud-Ansari, S.,
1007 Méndez, F.J., Murray, A.B., Plant, N.G., Ratliff, K.M., Robinet, A., Rueda, A., Sénéchal, N.,
1008 Simmons, J.A., Splinter, K.D., Stephens, S., Townend, I., Vitousek, S., Vos, K., 2020. Blind
1009 testing of shoreline evolution models, Scientific Reports, 10, 2137,
1010 https://doi.org/10.1038/s41598-020-59018-y.

1011 Montreuil, A.L., Levoy, F., Bretel, P., Anthony, E.J., 2014. Morphological diversity and
1012 complex sediment recirculation on the ebb delta of a macrotidal inlet (Normandy, France): a
1013 multiple LiDAR dataset approach. Geomorphology 219, 114-125.
1014 https://doi.org/10.1016/j.geomorph.2014.05.008.

1015 Ndour, A., Laïbi, R., Sadio, M., Degbé, C.D.E., Diaw, A.T., Oyédé, L.M., Anthony, E.J.,
1016 Dussouillez, P., Sambou, H., Dièye, E.H.B., 2018. Management strategies for coastal erosion
1017 problems in West Africa: Analysis, issues, and constraints drawn from examples from
1018 Senegal and Benin. Ocean Coast. Manag. 156, 92-106.
1019 https://doi.org/10.1016/j.ocecoaman.2017.09.001.

Nmiss, M., Anthony, E.J., Amyay, M., Ouammou, A., 2022. Multi-decadal shoreline change, inherited coastal morphology and sediment supply in the Souss-Massa littoral cell (Morocco), and a prognosis with sea-level rise. Journal of African Earth Sciences, 196, 104672. https://doi.org/10.1016/j.jafrearsci.2022.104672.

Pellerin Le Bas, X., Levoy, F., 2018. Bar migrations on a macrotidal ebb delta over a period of six years using Lidar survey. Journal of Coastal Research, Special Issue 85, 146-150. https://dx.doi.org/10.2112/SI85-030.1.

Pranzini, E., 2013. Coastal erosion and protection in Europe. Pranzini, E., Williams, A. (Eds), Routledge, London & New York.

Prime, T., 2018. Jersey sea level and coastal conditions climate review. National Oceanography Centre. 73 p.

Pye, K., Blott, S.J., 2008. Decadal-scale variation in dune erosion and accretion rates: An investigation of the significance of changing storm tide frequency and magnitude on the Sefton coast, UK. Geomorphology 102(3-4), 652-666. https://doi.org/10.1016/j.geomorph.2008.06.011.

Ranasinghe, R., 2016. Assessing climate change impacts on open sandy coasts: a review. Earth Sci. Rev. 160, 320-332. https://doi.org/10.1016/j.earscirev.2016.07.011.

Richter, A., Faust, D., Maas, H.G., 2013. Dune cliff erosion and beach width change at the northern and southern spits of Sylt detected with multi-temporal Lidar. Catena, 103, 103-111. https://doi.org/10.1016/j.catena.2011.02.007.

Robin, N., Levoy, F., 2007. Etapes et rythmes de formation d'une flèche sédimentaire à crochets multiples en environnement megatidal. *Zeitschrift für Geomorphologie* 51, 337-360. https://hal.archives-ouvertes.fr/hal-00196669.

Robin, N., Levoy, F., Monfort, O., 2007. Bar morphodynamic behaviour on the ebb delta of a macrotidal inlet (Normandy, France). J. Coastal Res. 23, 1370-1378. https://doi.org/10.2112/06-0684.1.

Robin, N., Levoy, F., Monfort, O., 2009a. Short term morphodynamics of an intertidal bar on megatidal ebb delta. Marine Geology 260(1-4), 102-120. https://dx.doi.org/10.1016/j.margeo.2009.02.006.

Robin, N., Levoy, F., Monfort, O., Anthony, E.J., 2009b. Short-term to multi-decadal scale onshore bar migration and shoreline changes in the vicinity of a megatidal ebb delta. Journal of Geophysical Research 114, F04024. https://doi.org/10.1029/2008JF001207.

Robin, N., Levoy, F., Anthony, E.J., Monfort, O., 2020. Sand spit dynamics in a large tidal-range environment: Insight from multiple LiDAR, UAV and hydrodynamic measurements on multiple spit hook development, breaching, reconstruction, and shoreline changes. Earth Surf. Process. Landforms 45, 2706-2726. http://dx.doi.org/10.1002/esp.4924.

Sánchez-Arcilla, A., Jiménez, J.A., 1994. Breaching in a wave-dominated barrier spit: the Trabucador bar (northeastern Spanish coast). Earth Surface Processes and Landforms 19, 483-498. https://doi.org/10.1002/esp.3290190602.

1059 Sarti, G., Bertoni, D., Bini, M., 2022. Integrating different databases to offer a geological
1060 perspective of coastal management: A review case from the Northern Tuscany littoral cell
1061 (Italy). J. Mar. Sci. Eng., 10(3), 353. https://doi.org/10.3390/jmse10030353.

1062 Saye, S.E., Van der Wal, D., Pye, K., Blott, S.J., 2005. Beach-dune morphological
1063 relationships and erosion/accretion: An investigation at five sites in England and Wales using
1064 LIDAR data. Geomorphology, 72(1-4), 128-155.
1065 https://doi.org/10.1016/j.geomorph.2005.05.007.

1066 SHOM, 2022. Références Altimétriques Maritimes, Ports de France métropolitaine et d'outre-
1067 mer. ISBN 978-2-11-139505-3, 121 p.

1068 Slott, J.M., Murray, A.B., Ashton, A.D., 2010. Large-scale responses of complex-shaped
1069 coastlines to local shoreline stabilization and climate change. Journal of Geophysical
1070 Research 115, F03033. https://doi.org/10.1029/2009JF001486.

1071 Stive, M.J., Aarninkhof, S.G., Hamm, L., Hanson, H., Larson, M., Wijnberg, K.M., Nicholls,
1072 R.J., Capobianco, M., 2002. Variability of shore and shoreline evolution. Coast. Eng. 47(2),
1073 211-235. https://doi.org/10.1016/S0378-3839(02)00126-6.

1074 Stive, M.J.F., 2004. How important is global warming for coastal erosion? Climate Change
1075 64, 27-39. https://doi.org/10.1023/B:CLIM.0000024785.91858.1d.

1076 Stockdon, H.F., Doran, K.S., Sallenger, A.H., 2009. Extraction of lidar-based dune-crest
1077 elevations for use in examining the vulnerability of beaches to inundation during hurricanes.
1078 Journal of Coastal Research, SI 53, 59-65. https://doi.org/10.2112/SI53-007.1.

1079 Syvitski, J., Ángel, J.R., Saito, Y., Overeem, I., Vorosmarty, C., Wang, H., Olago, D., 2022.
1080 Earth's sediment cycle during the Anthropocene. Nat. Rev. Earth Environ. 3, 179-196.
1081 https://doi.org/10.1038/s43017-021-00253-w

1082 Thieler, E.R., Himmelstoss, E.A., Zichichi, J.L., Ayhan, E., 2009. Digital Shoreline Analysis
1083 System (DSAS) version 4.2, An ArcGIS extension for calculating shoreline changes. U.S.
1084 Geological Survey Open-File Report, 2008-1278.

1085 Thomas, C.W., Murray, A.B., Ashton, A.D., Hurst, M.D., Barkwith, A.K.A.P., Ellis, M.A.,
1086 2016. Complex coastlines responding to climate change: do shoreline shapes reflect present
1087 forcing or "remember" the distant past? Earth Surf. Dynam. 4, 871-884.
1088 https://doi.org/10.5194/esurf-4-871-2016.

1089 Turki, I., Massei, N., Laignel, B., Shafiei, H., 2020. Effects of global climate oscillations on
1090 intermonthly to interannual variability of sea levels along the English channel coasts (NW
1091 France). Oceanologia, 62(2), 226-242. https://doi.org/10.1016/j.oceano.2020.01.001.

1092 Uda, T., 2010. Japan's Beach Erosion; Reality and Future Measures, World Scientific,
1093 Singapore, 418 pp. http://dx.doi.org/10.1142/7332.

1094 van Rijn, L.C., 1990. Principles of Fluid Flow and Surface Waves in Rivers, Estuaries, Seas
1095 and Oceans. Aqua Publications, Odemarked, The Netherlands., 343 pp.

Vos, K., Harley, M.D., Splinter, K.D., Simmons, J.A., Turner, I.L., 2019. Sub-annual to multi-decadal shoreline variability from publicly available satellite imagery. Coast. Eng. 150, 160-174. https://doi.org/10.1016/j.coastaleng.2019.04.004.

Vousdoukas, M.I., Ranasinghe, R., Mentaschi, L., Plomartis, T.A., Athanasiou, P., Luijendyk, A., Feyen, L., 2020. Sandy Beaches under threat of erosion. Nat. Clim. Change 10, 260-263.

Wijnberg, K.M., Terwindt, J.H.J., 1995. Extracting decadal morphological behaviour from high-resolution, long-term bathymetric surveys along the Holland coast using eigenfunction analysis. Marine Geology 126, 301-330. https://doi.org/10.1016/0025-3227(95)00084-C.

Zăinescu, F.J., Vespremenu-Stroe, A., Tătui, F., 2019. The formation and closure of the big breach of Sacalin spit associated with extreme shoreline retreat and shoreface erosion. Earth Surface Processes and Landforms 44(11), 2268-2284. https://doi.org/10.1002/esp.4639.

Zhang, K., Douglas, B.C., Leatherman, S.P., 2004. Global Warming and Coastal Erosion. Climatic Change 64, 41. https://doi.org/10.1023/B:CLIM.0000024690.32682.48.

Fig. 1: Map of the Cotentin Peninsula showing the study area (red zone) and the Channel Islands embayment between Normandy and Brittany, northern France (purple circles indicate land- and sea-level measurement locations).

Fig. 2: Locations of shoreline survey points, HOMERE wave model outputs and wave measurements along the west Cotentin coast. The green arrows indicate residual longshore sediment transport directions (from Levoy, 1994).

Fig. 3: Locations of anthropogenic actions on the west Cotentin shoreline (hard engineering structures and beach or dune-front nourishments).

Fig. 4: Shoreline changes between 1992 and 2019: (A) heatmap showing spatial and temporal variability of change (grey bars = no data available); (B) Net Shoreline Movement; (C) locations of shoreline surveys (in red, survey locations with an ebb delta spatial footprint); (D) End Point Rate.

Fig. 5: Tree-view of the main Shoreline Temporal Change Signature (STCS) clusters, non-dimensional change envelops (grey surface), and averages (red line) for each of the clusters (A to I). NDC = Non-dimensional change.

Fig. 6: Locations of shoreline surveys and their associated STCS clusters (A to I). Note that survey locations SW161, SW162 and SW44 are not included in the cluster analysis due to shorter survey durations.

Fig. 7: Annual mean sea levels at the port of Saint-Malo relative to local datum over the period 1995-2019, and the long-term trend.

Fig. 8: Fluctuations in the annual number of events from 1994 to 2016 coupling high-tide water levels exceeding the mean spring-tide water level and wave heights > 1 m for HOMERE locations along the west Cotentin coast.

Fig. 9. Mean wave energy flux during winter months between 1994/1995 and 2015/2016 and for high tide water levels exceeding the mean spring-tide water level.

Fig. 10: Evolution of the winter (December-March) NAO index (A), and the WEPA index (B).

Fig. 11: Correlation between the mean wave energy flux during winter months on the west Cotentin coast and the winter NAO index (A) and WEPA index (B) between 1995 and 2016 (the latter significant at the 99% level).

Fig. 12: Order of magnitude of vertical ranges of sea-level rise, spring high tides, storm surges, wave run-up and beach elevation affecting shoreline mobility on the sandy west Cotentin coast over the last three decades.

Fig. 13: Non-dimensional coastline location change (in blue) for the 9 identified clusters and mean and annual mean sea levels at the port of Saint-Malo (in red).

Fig. 14: Non-dimensional coastline location change (in blue) for the 9 identified clusters and mean wave energy flux during winter months (in red).

Fig. 15: Computed energy flux from wave data between 1994 and 2016 and extrapolated between 1950 and 2019, showing the long-term trend of wave activity along the west Cotentin coast during tide levels exceeding mean spring high tides.

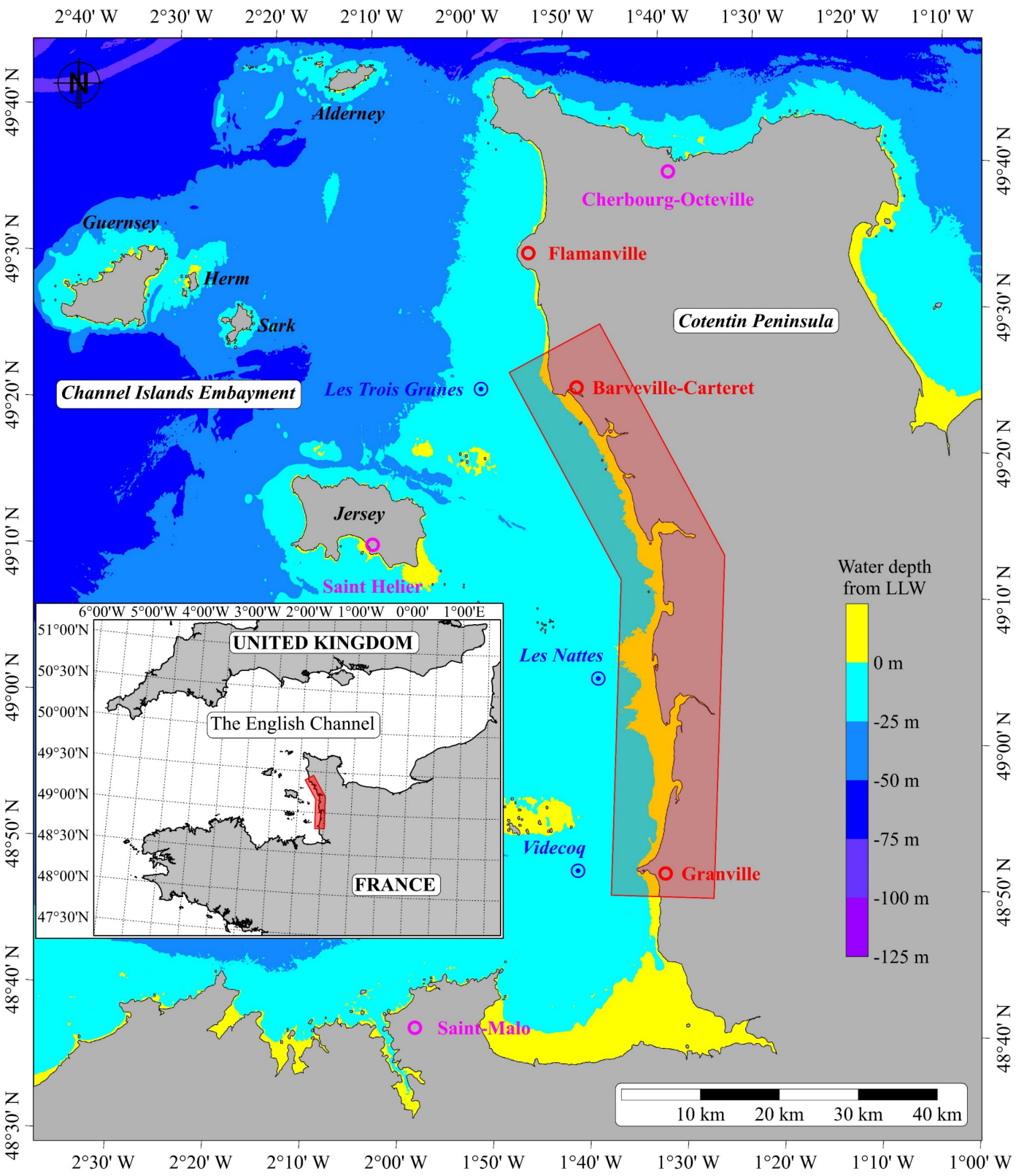
2°40' W
2°30' W
2°20' W
2°10' W
2°00' W
1°50' W
1°40' W
1°30' W
1°20' W
1°10' W
1°00' W
49°40' N
49°30' N
49°20' N
49°10' N
49°00' N
48°50' N
48°40' N
48°30' N
Alderney
Guernsey
Herm
Sark
Channel Islands Embayment
Les Trois Grunes
Jersey
Saint Helier
Cherbourg-Octeville
Flamanville
Cotentin Peninsula
Barveville-Carteret
Les Nattes
Videcoq
Granville
Saint-Malo
Water depth from LLW
0 m
-25 m
-50 m
-75 m
-100 m
-125 m
10 km
20 km
30 km
40 km
6°00'W 5°00'W 4°00'W 3°00'W 2°00'W 1°00'W 0°00' 1°00'E
51°00'N
50°30'N
50°00'N
49°30'N
49°00'N
48°30'N
48°00'N
47°30'N
UNITED KINGDOM
The English Channel
FRANCE

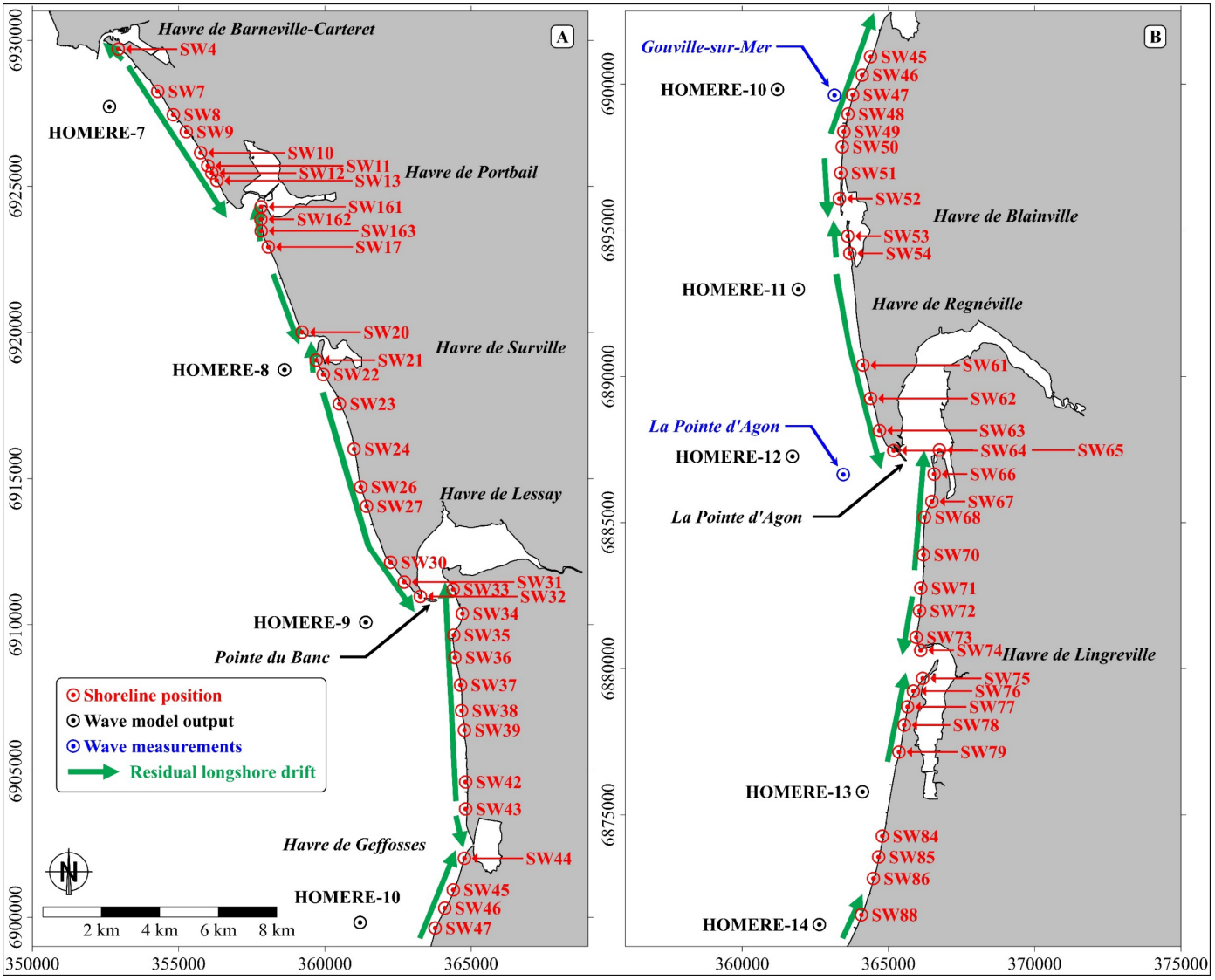
A
B
Havre de Barneville-Carteret
Havre de Portbail
Havre de Surville
Havre de Lessay
Havre de Geffosses
Havre de Blainville
Havre de Regnéville
Havre de Lingreville
Gouville-sur-Mer
La Pointe d'Agon
Pointe du Banc
HOMERE-7
HOMERE-8
HOMERE-9
HOMERE-10
HOMERE-11
HOMERE-12
HOMERE-13
HOMERE-14
SW4
SW7
SW8
SW9
SW10
SW11
SW12
SW13
SW161
SW162
SW163
SW17
SW20
SW21
SW22
SW23
SW24
SW26
SW27
SW30
SW31
SW32
SW33
SW34
SW35
SW36
SW37
SW38
SW39
SW42
SW43
SW44
SW45
SW46
SW47
SW48
SW49
SW50
SW51
SW52
SW53
SW54
SW61
SW62
SW63
SW64
SW65
SW66
SW67
SW68
SW70
SW71
SW72
SW73
SW74
SW75
SW76
SW77
SW78
SW79
SW84
SW85
SW86
SW88
Shoreline position
Wave model output
Wave measurements
Residual longshore drift
N
2 km
4 km
6 km
8 km
6930000
6925000
6920000
6915000
6910000
6905000
6900000
6900000
6895000
6890000
6885000
6880000
6875000
350000
355000
360000
365000
360000
365000
370000
375000

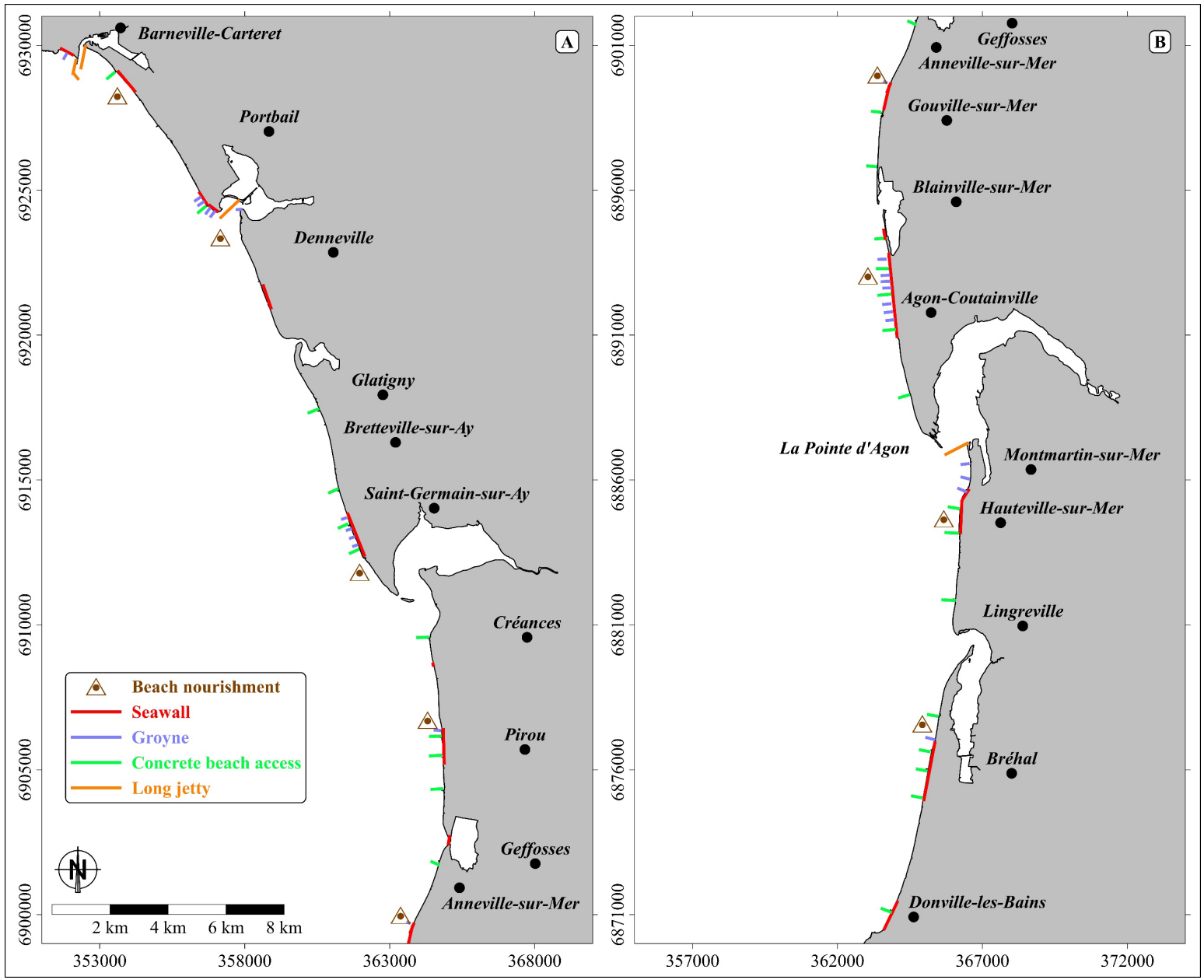
A
B
Barneville-Carteret
Portbail
Denneville
Glatigny
Bretteville-sur-Ay
Saint-Germain-sur-Ay
Créances
Pirou
Geffosses
Anneville-sur-Mer
Geffosses
Anneville-sur-Mer
Gouville-sur-Mer
Blainville-sur-Mer
Agon-Coutainville
La Pointe d'Agon
Montmartin-sur-Mer
Hauteville-sur-Mer
Lingreville
Bréhal
Donville-les-Bains
Beach nourishment
Seawall
Groyne
Concrete beach access
Long jetty
N
2 km
4 km
6 km
8 km
6930000
6925000
6920000
6915000
6910000
6905000
6900000
6901000
6896000
6891000
6886000
6881000
6876000
6871000
353000
358000
363000
368000
357000
362000
367000
372000

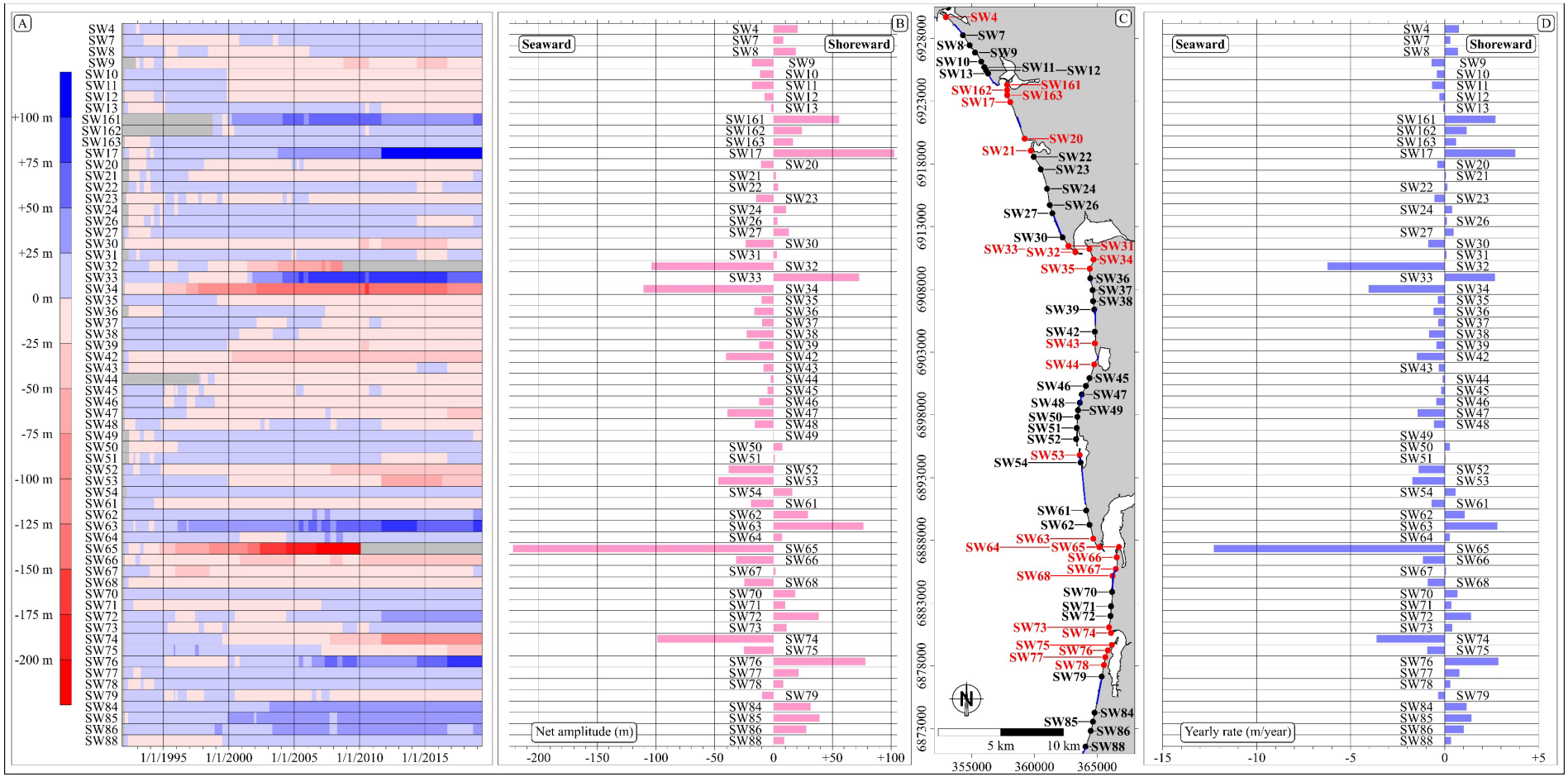
A
B
C
D
Seaward
Shoreward
+100 m
+75 m
+50 m
+25 m
0 m
-25 m
-50 m
-75 m
-100 m
-125 m
-150 m
-175 m
-200 m
1/1/1995
1/1/2000
1/1/2005
1/1/2010
1/1/2015
Net amplitude (m)
-200
-150
-100
-50
0
+50
+100
6928000
6923000
6918000
6913000
6908000
6903000
6898000
6893000
6888000
6883000
6878000
6873000
355000
360000
365000
5 km
10 km
N
Yearly rate (m/year)
-15
-10
-5
0
+5

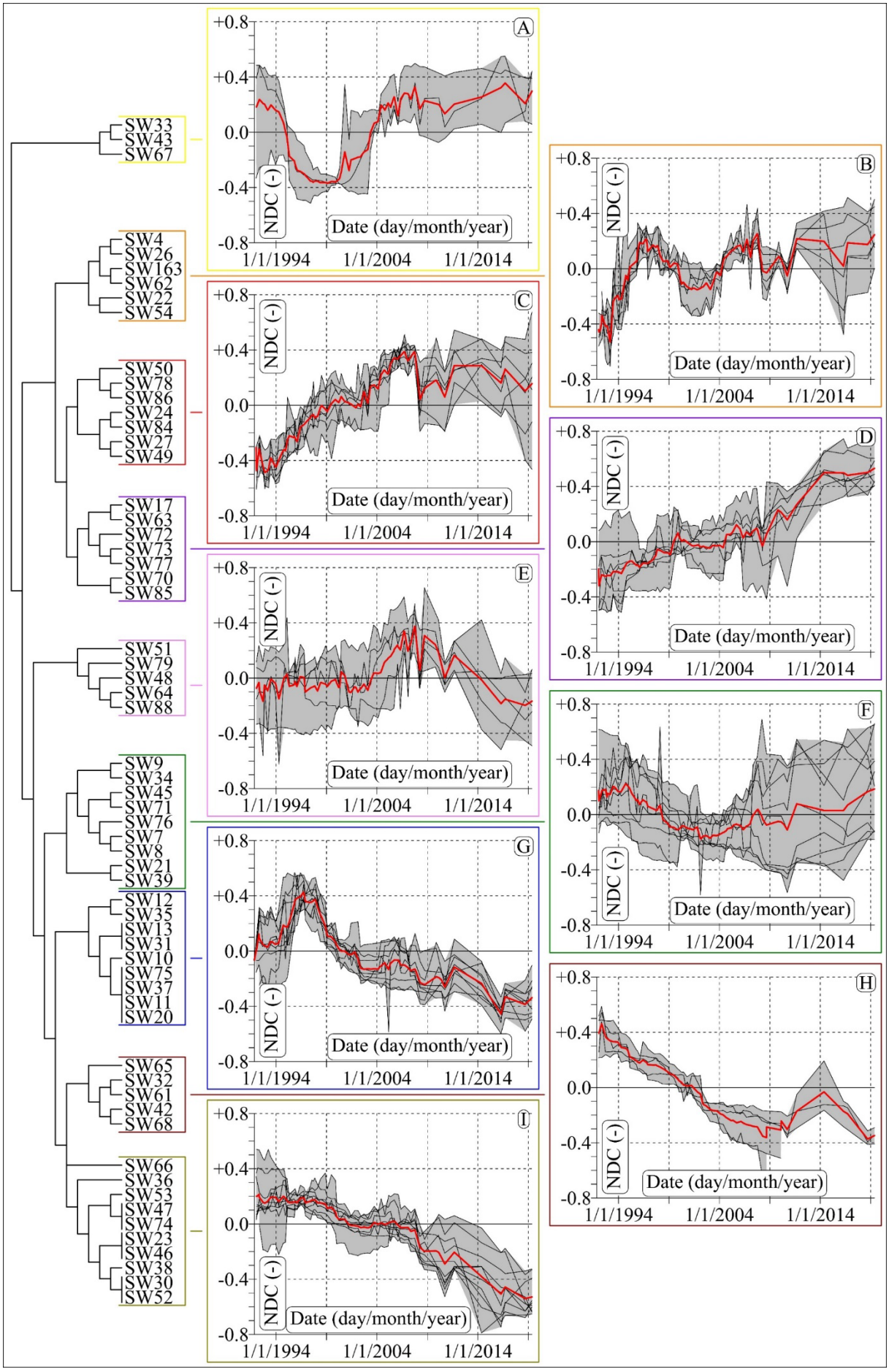
SW33
SW43
SW67
SW4
SW26
SW163
SW62
SW22
SW54
SW50
SW78
SW86
SW24
SW84
SW27
SW49
SW17
SW63
SW72
SW73
SW77
SW70
SW85
SW51
SW79
SW48
SW64
SW88
SW9
SW34
SW45
SW71
SW76
SW7
SW8
SW21
SW39
SW12
SW35
SW13
SW31
SW10
SW75
SW37
SW11
SW20
SW65
SW32
SW61
SW42
SW68
SW66
SW36
SW53
SW47
SW74
SW23
SW46
SW38
SW30
SW52
A
B
C
D
E
F
G
H
I
+0.8
+0.4
0.0
-0.4
-0.8
NDC (-)
Date (day/month/year)
1/1/1994
1/1/2004
1/1/2014

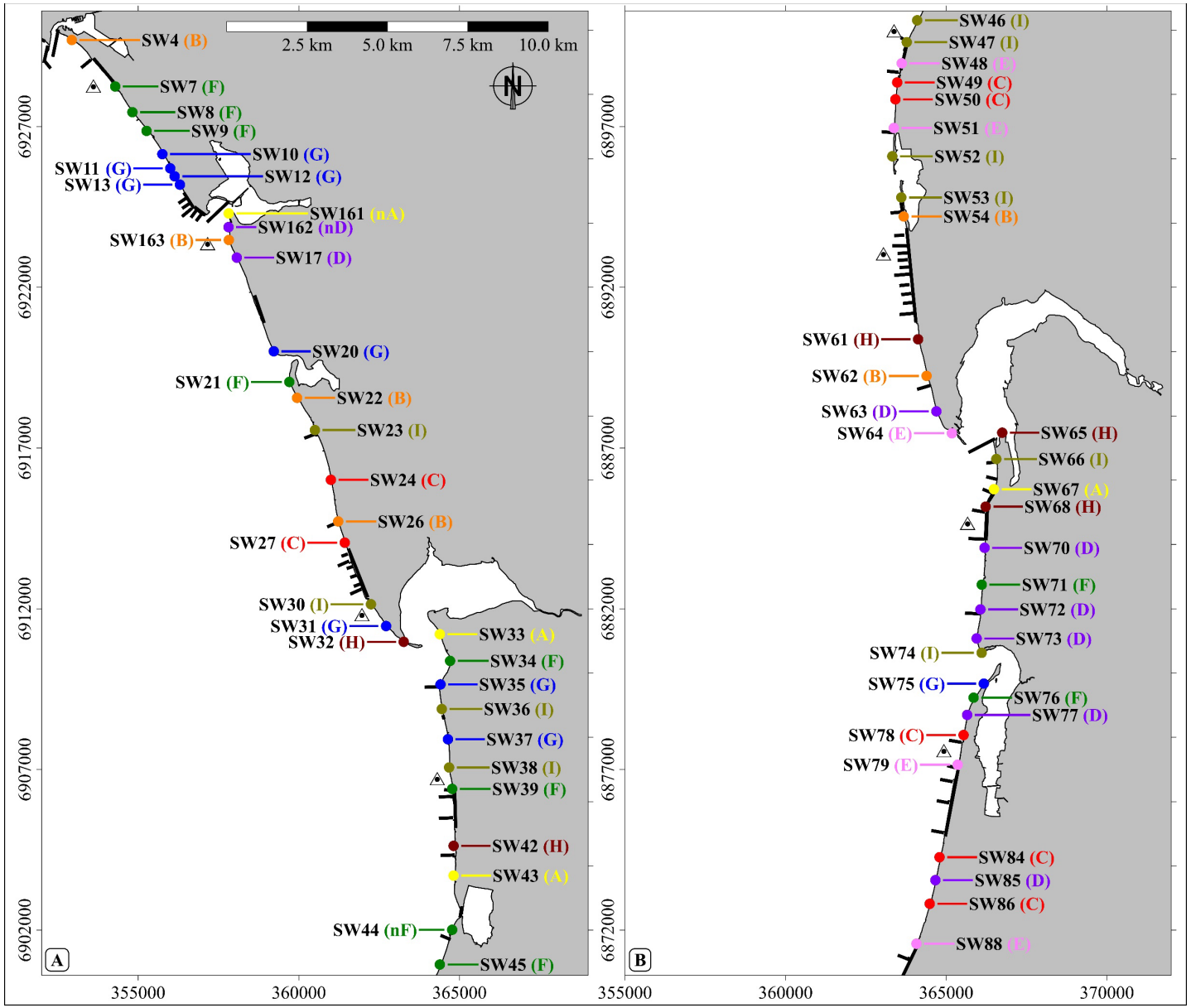
2.5 km
5.0 km
7.5 km
10.0 km
N
SW4 (B)
SW7 (F)
SW8 (F)
SW9 (F)
SW10 (G)
SW11 (G)
SW12 (G)
SW13 (G)
SW161 (nA)
SW162 (nD)
SW163 (B)
SW17 (D)
SW20 (G)
SW21 (F)
SW22 (B)
SW23 (I)
SW24 (C)
SW26 (B)
SW27 (C)
SW30 (I)
SW31 (G)
SW32 (H)
SW33 (A)
SW34 (F)
SW35 (G)
SW36 (I)
SW37 (G)
SW38 (I)
SW39 (F)
SW42 (H)
SW43 (A)
SW44 (nF)
SW45 (F)
A
6927000
6922000
6917000
6912000
6907000
6902000
355000
360000
365000
SW46 (I)
SW47 (I)
SW48 (E)
SW49 (C)
SW50 (C)
SW51 (E)
SW52 (I)
SW53 (I)
SW54 (B)
SW61 (H)
SW62 (B)
SW63 (D)
SW64 (E)
SW65 (H)
SW66 (I)
SW67 (A)
SW68 (H)
SW70 (D)
SW71 (F)
SW72 (D)
SW73 (D)
SW74 (I)
SW75 (G)
SW76 (F)
SW77 (D)
SW78 (C)
SW79 (E)
SW84 (C)
SW85 (D)
SW86 (C)
SW88 (E)
B
6897000
6892000
6887000
6882000
6877000
6872000
355000
360000
365000
370000

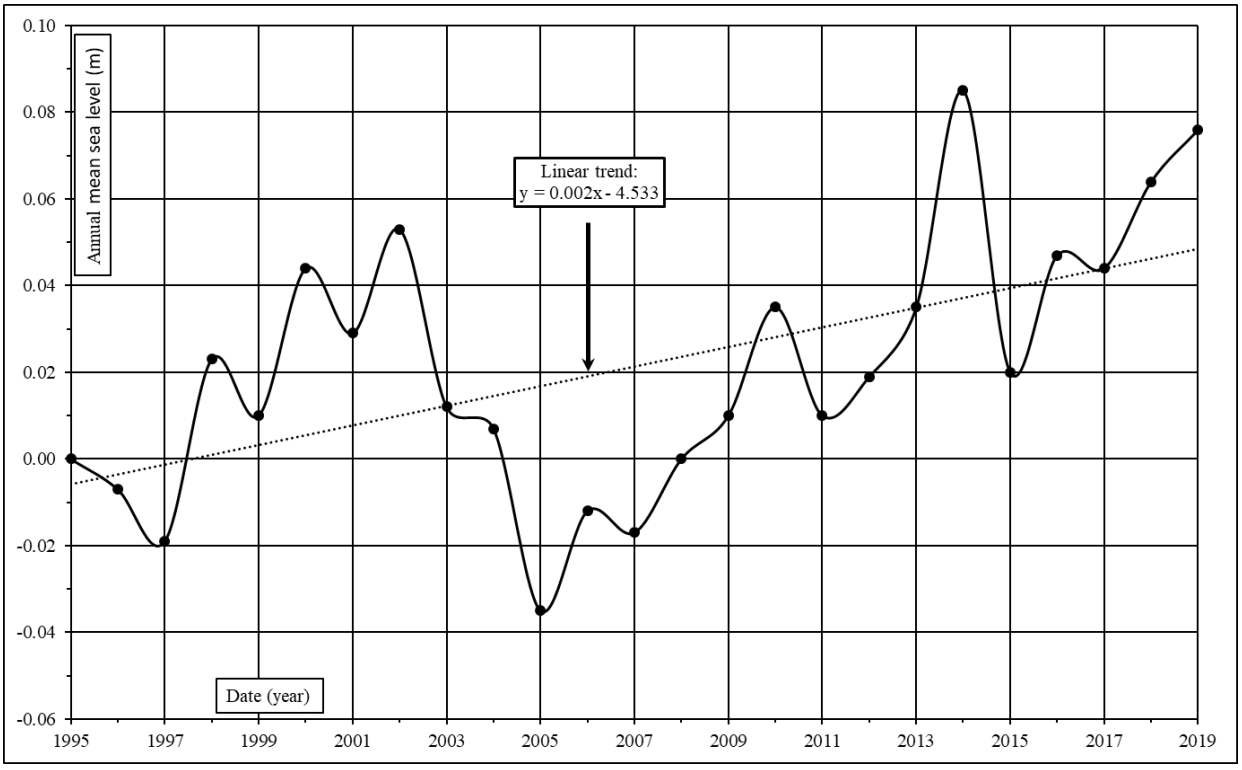
Annual mean sea level (m)
Linear trend:
y = 0.002x - 4.533
Date (year)
0.10
0.08
0.06
0.04
0.02
0.00
-0.02
-0.04
-0.06
1995
1997
1999
2001
2003
2005
2007
2009
2011
2013
2015
2017
2019

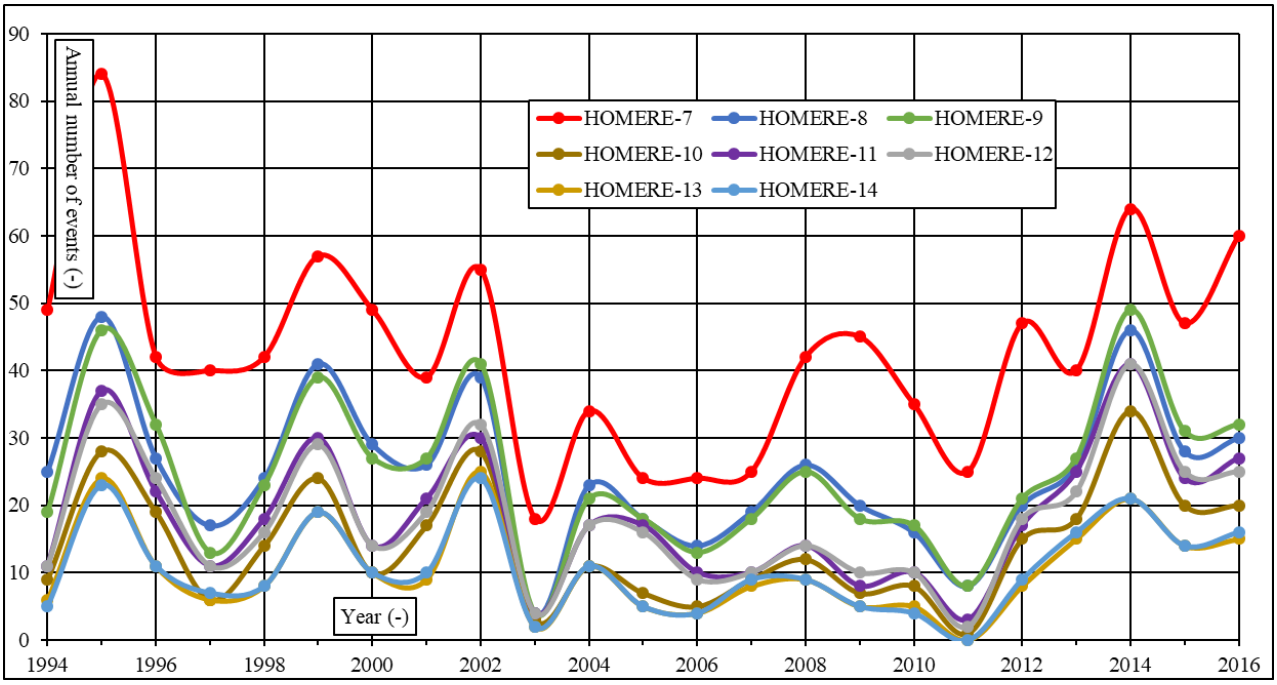
Annual number of events (-)
HOMERE-7
HOMERE-8
HOMERE-9
HOMERE-10
HOMERE-11
HOMERE-12
HOMERE-13
HOMERE-14
Year (-)
0
10
20
30
40
50
60
70
80
90
1994
1996
1998
2000
2002
2004
2006
2008
2010
2012
2014
2016

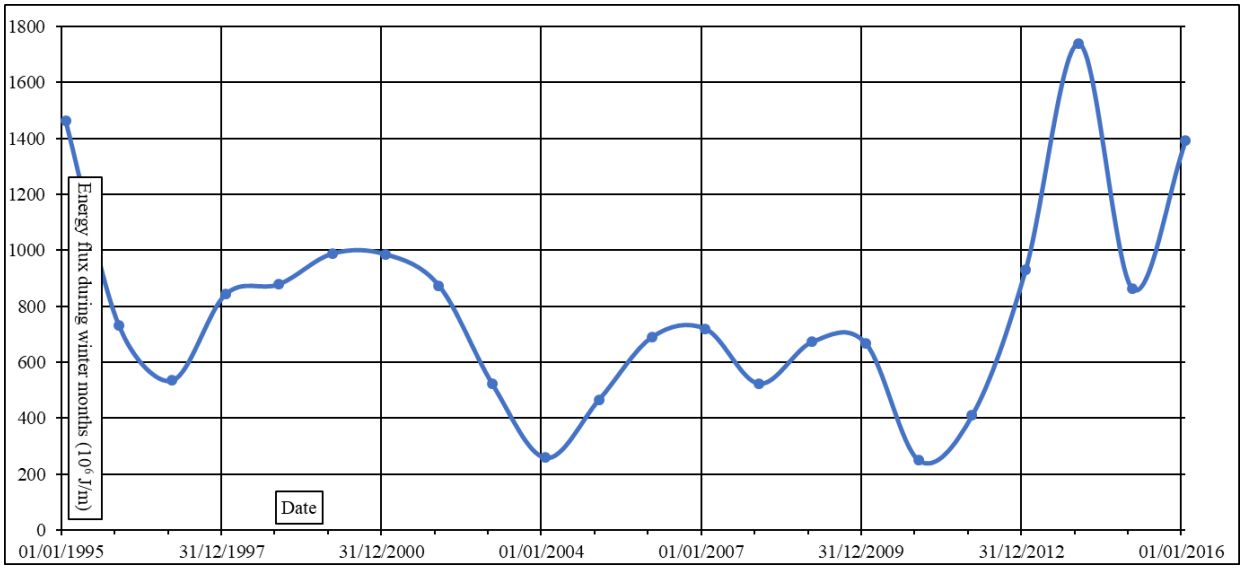
1800
1600
1400
1200
1000
800
600
400
200
0
Energy flux during winter months (10^6 J/m)
Date
01/01/1995
31/12/1997
31/12/2000
01/01/2004
01/01/2007
31/12/2009
31/12/2012
01/01/2016

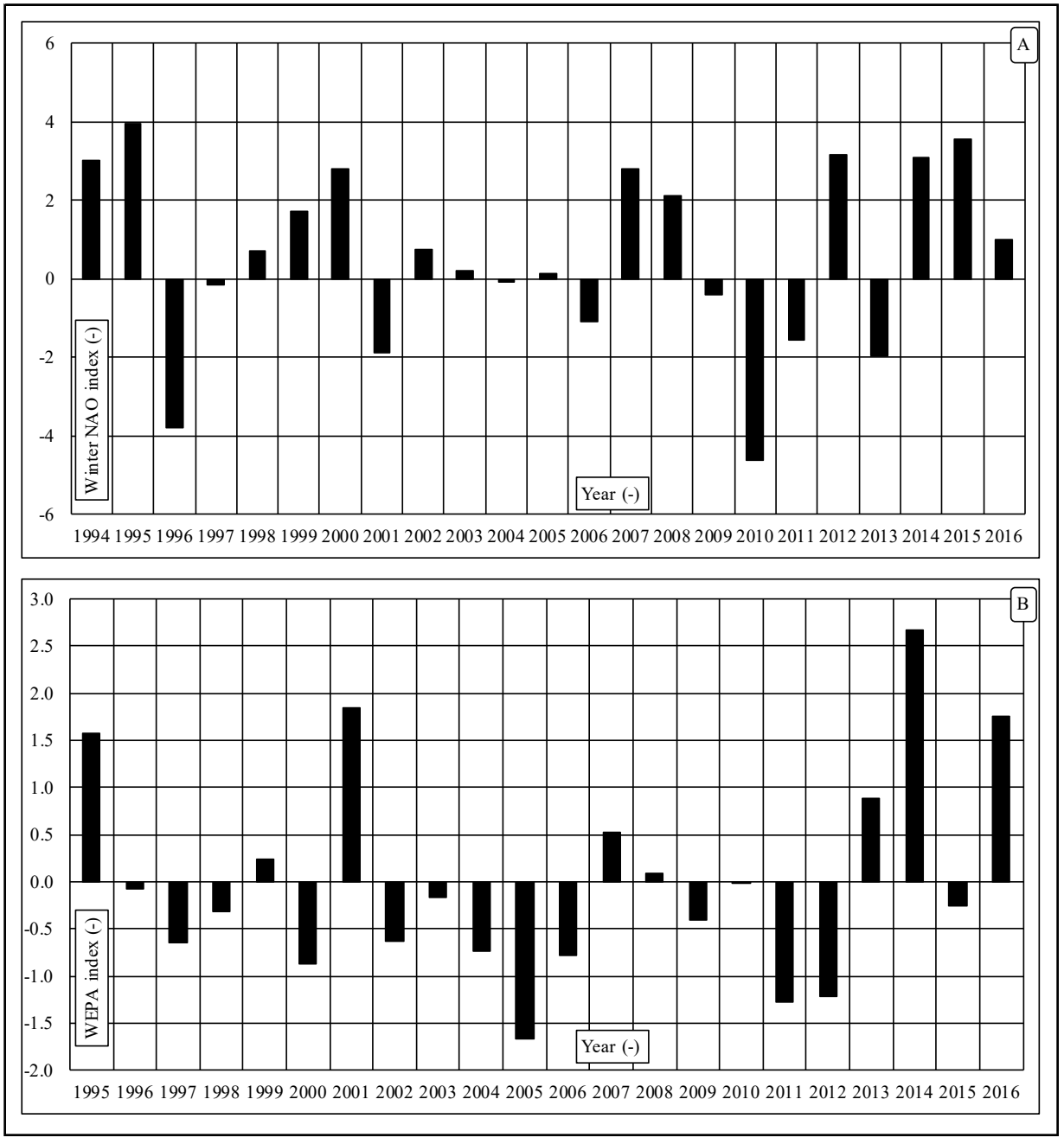
A
6
4
2
0
-2
-4
-6
Winter NAO index (-)
Year (-)
1994 1995 1996 1997 1998 1999 2000 2001 2002 2003 2004 2005 2006 2007 2008 2009 2010 2011 2012 2013 2014 2015 2016
B
3.0
2.5
2.0
1.5
1.0
0.5
0.0
-0.5
-1.0
-1.5
-2.0
WEPA index (-)
Year (-)
1995 1996 1997 1998 1999 2000 2001 2002 2003 2004 2005 2006 2007 2008 2009 2010 2011 2012 2013 2014 2015 2016

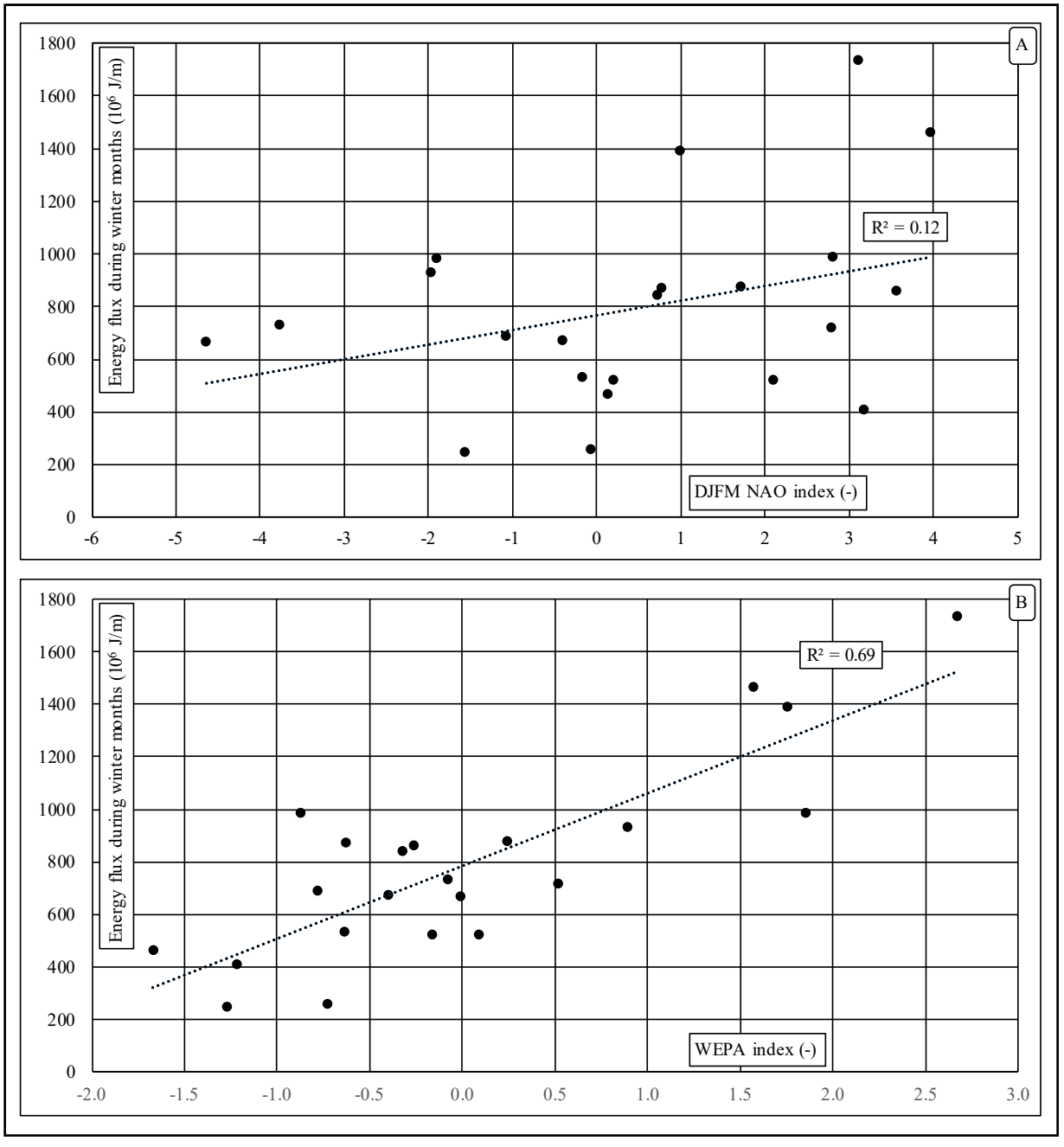
A
Energy flux during winter months (10⁶ J/m)
1800
1600
1400
1200
1000
800
600
400
200
0
-6
-5
-4
-3
-2
-1
0
1
2
3
4
5
R² = 0.12
DJFM NAO index (-)
B
Energy flux during winter months (10⁶ J/m)
1800
1600
1400
1200
1000
800
600
400
200
0
-2.0
-1.5
-1.0
-0.5
0.0
0.5
1.0
1.5
2.0
2.5
3.0
R² = 0.69
WEPA index (-)

Mean sea level
(Saint-Malo)

Long-term trend

+0.002 m/y

Interannual variability range

0.12 m

High tide level variations

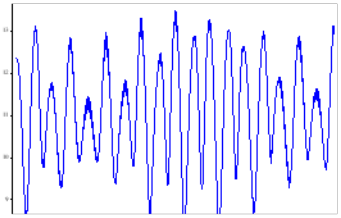

Range between mean and exceptional spring high tide levels

Up to 1.59 m

Including effects of:

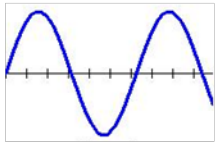

18.6 y nodal lunar cycle

Up to 0.3 m

Observed storm surges

Up to 1.6 m

Measured wave run-up*

Up to 3 m

Beach/Dune morphology & elevation changes

Up to 2.8 m

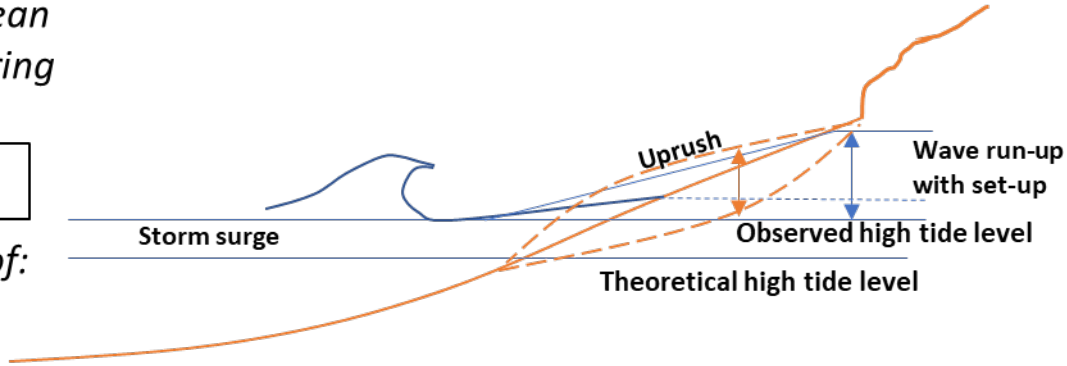

*Including wave set-up

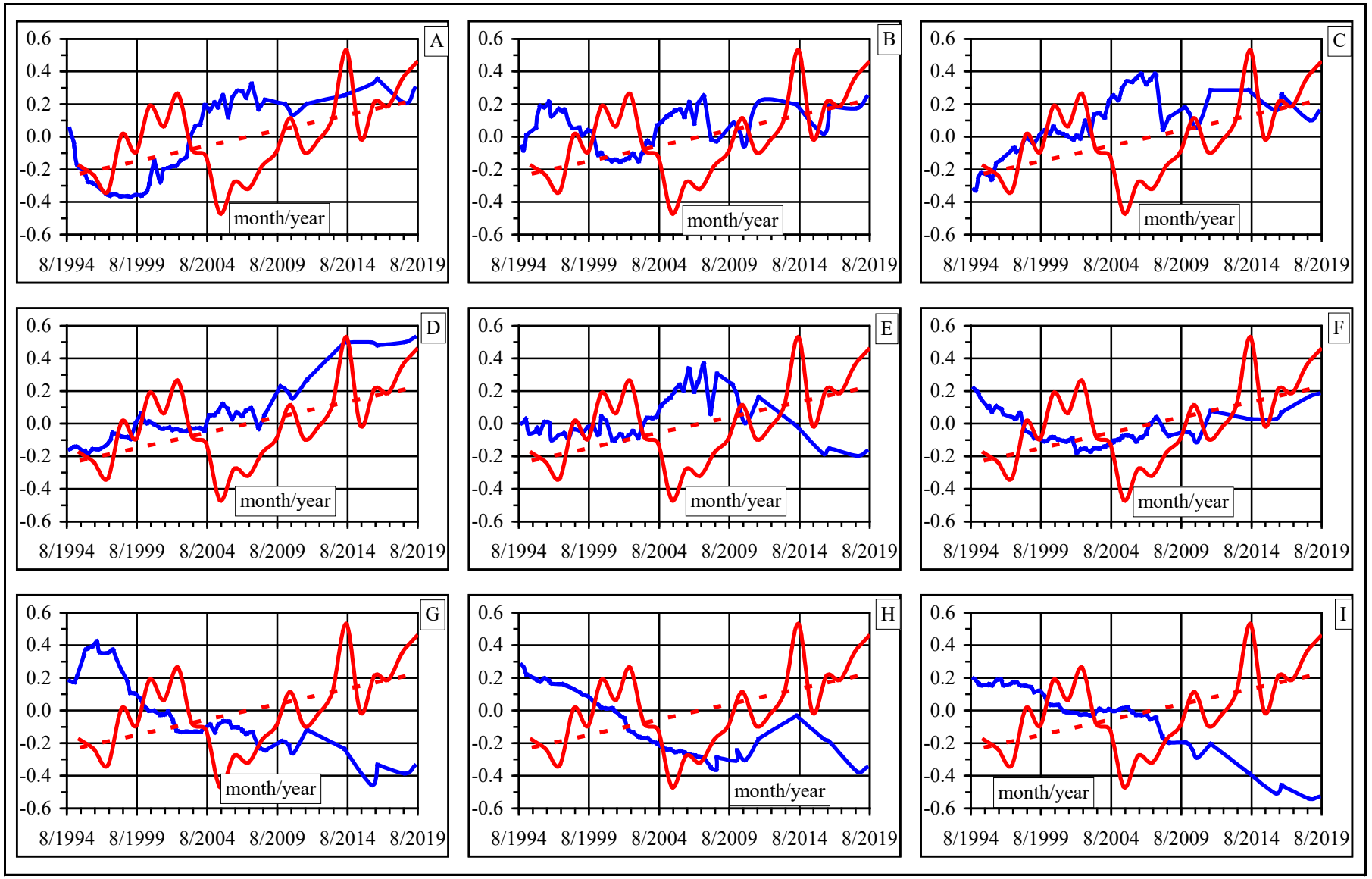
A
B
C
D
E
F
G
H
I
0.6
0.4
0.2
0.0
-0.2
-0.4
-0.6
8/1994
8/1999
8/2004
8/2009
8/2014
8/2019
month/year

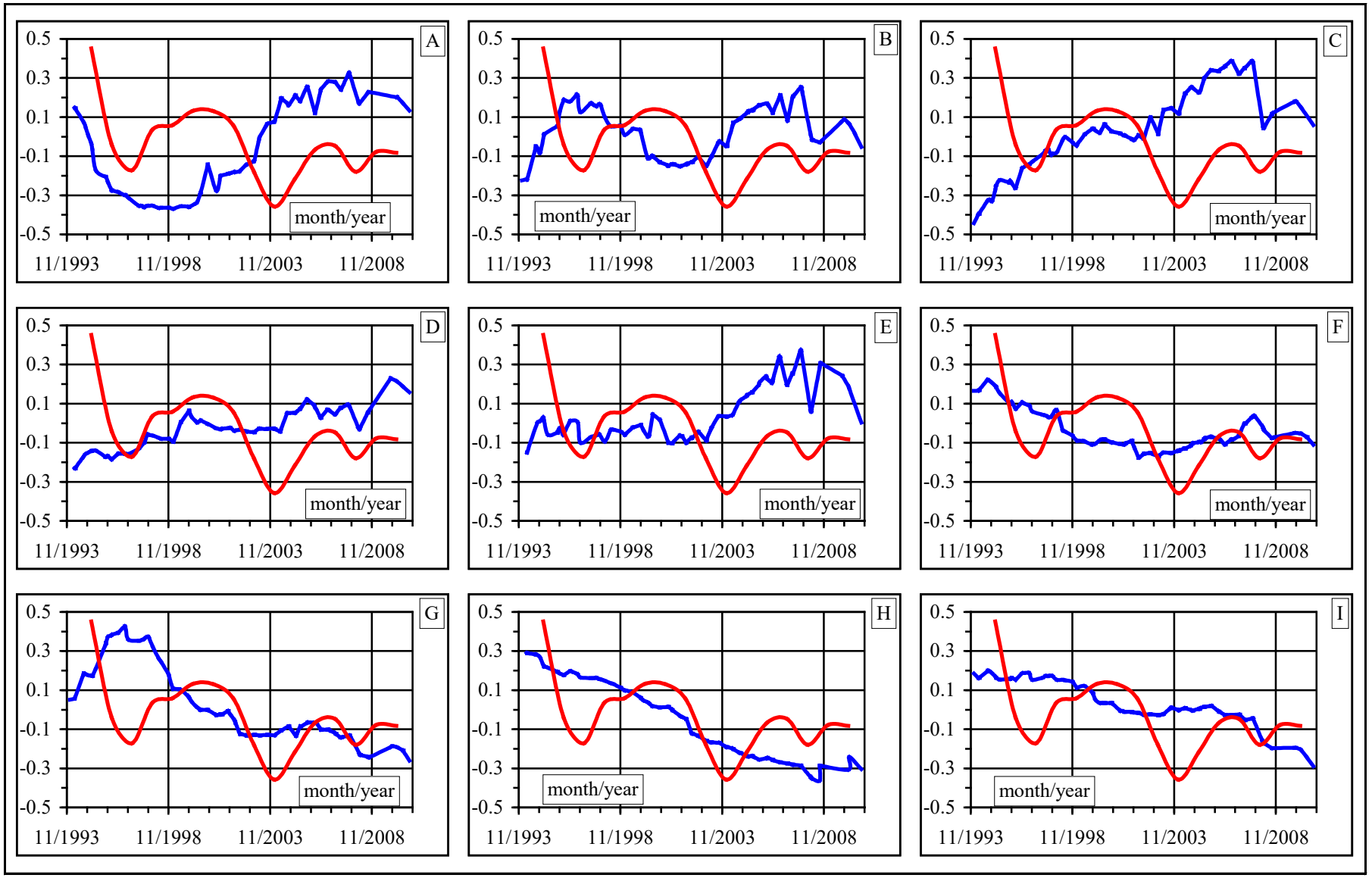
A
B
C
D
E
F
G
H
I
0.5
0.3
0.1
-0.1
-0.3
-0.5
11/1993
11/1998
11/2003
11/2008
month/year

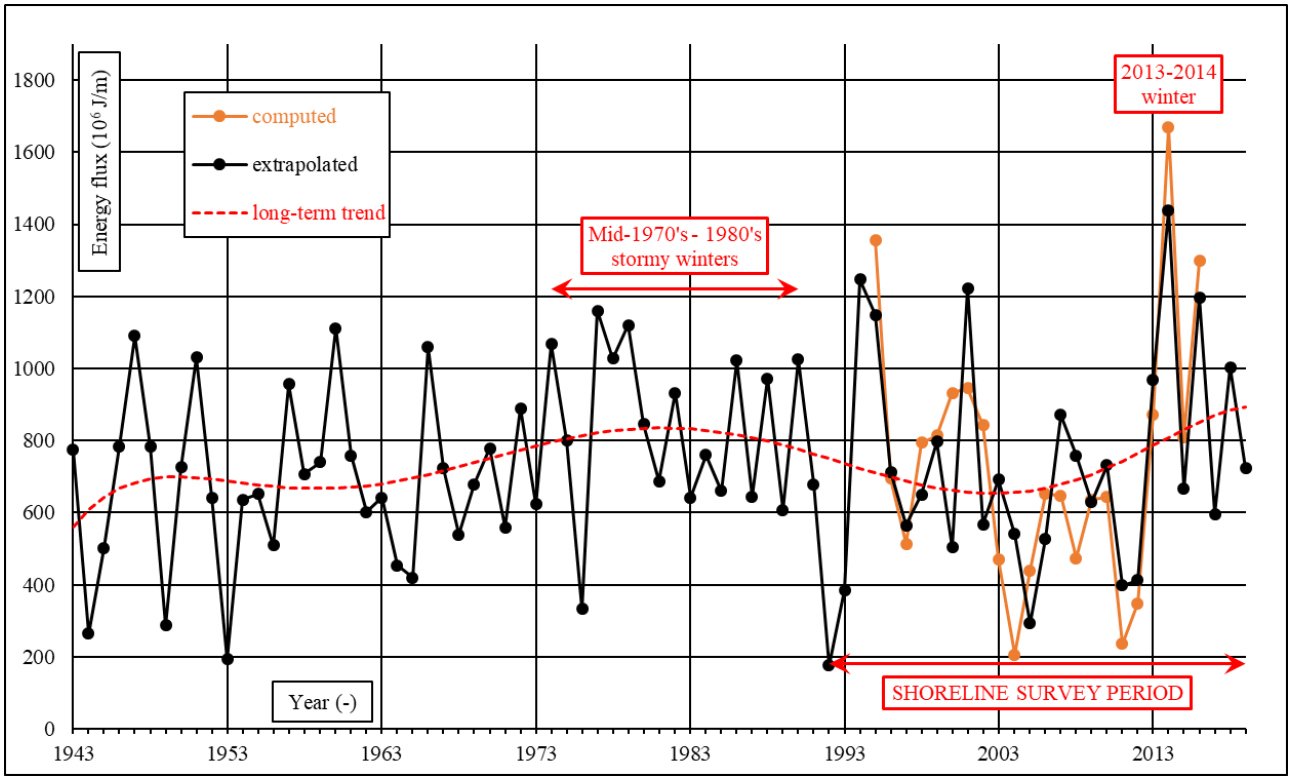
Energy flux (10^6 J/m)
computed
extrapolated
long-term trend
Mid-1970's - 1980's
stormy winters
2013-2014
winter
SHORELINE SURVEY PERIOD
Year (-)
0
200
400
600
800
1000
1200
1400
1600
1800
1943
1953
1963
1973
1983
1993
2003
2013

Survey number	Survey dates	Sources
1	21 September 2009	CLAREC project
2	22 September 2010	CLAREC project
3	31 August and 1st September 2011	CLAREC project
4	14 and 15 May 2014	CLAREC project
5	20 April 20 2016	CLAREC project
6	17 September 2016	ROLNP project
7	9 May 2017	CLAREC project
8	11 September 2018	COZULIT project
9	16 May 2019	COZULIT project

Table 1: LiDAR campaigns along the west Cotentin coast and the associated survey projects between 2009 and 2019.

Dates	Water level at high tide above the lowest predicted water level in Granville (m) (a)	Difference between observed and predicted high water levels in Granville (m) (b)	Difference between observed water level at high tide and the mean spring tide level (12.85 m in Granville) (m) (a+b)-12.85	Wind direction	Max wind speed (km/h)	Observations: (R): Large shoreline retreat (F): Flooding (B): Breaching (L): Beach lowering (P): Damage to coastal protection works
5-9 April 1962	13.65	+0.45	+1.25	SW	90 to 150	(R), (F)
1st March 1967	12.9	+0.2	+0.25	SW	90	(R), (P), (F)
1-2 Nov. 1967	13.9	+0.4	+1.45	W	130	(R), (F), (P), (B)
Feb. 1970	-	-	-	W	-	(R)
18 Jan. 1972	12.7	-	-			(R), (B), (P)
10 Jan. 1974	13.75	-	-	SSW	106	(R), (F)
6 Feb. 1974	14.1	-	-		Up to 180	(R), (L), (F)
11-12 Jan. 1978	13.7	+0.4	+1.25	N	Up to 140	(R), (P)
31 Jan.- 1 Feb. 1983	13.35	+0.35	+0.85	-	>120	(R)
19-20 Feb. 1984	13.9	+0.1	+1.15		-	(R), (F), (P)
23-24 Nov. 1984	13.45	+0.45	+1.05	SSW to WSW	150	(R), (B), (F)
6 April	14	+0.4	+1.55	S to SW	60	(R), (F)

1985						
6-9 Oct. 1987	13.75	+0.45	+1.35	SW to NW	87 to 102, up to 133	(R), (P), (L)
20-23 Jan. 1988	13.5	+0.6	+1.25	NW	130 to 158	(R), (F), (P), (L),
11-12 Feb. 1990	13.1	+0.4	+0.65		150	(R), (P)
26-28 Feb. 1990	13.65	+0.65	+1.45	SW	140	(R), (P), (L), (F)
23-24 Dec. 1999	13.35	+0.55	+1.05	SSW	130	(R)
31 March 2006	14.15	+0.15	+1.45	WNW	-	(R)
9-10 March 2008	13.7	-	-	WNW	123	(R), (B), (P), (F)
31 March 2010	13.9	-	-	W	90	(R), (P)

Table 2: Characteristics of the main historical storms that hit the west Cotentin coast between 1962 and 2010 resulting in shoreline retreat and coastal damages.